SEA STATE FORECASTING IN THE ST. LAWRENCE RIVER AND GULF

Ray Q. Lin and Will Perrie

Ocean Sciences Division
Maritimes Region
Fisheries and Oceans Canada

Bedford Institute of Oceanography
P.O. Box 1006
Dartmouth, Nova Scotia
Canada B2Y 4A2

1999

Canadian Technical Report of Hydrography and Ocean Sciences 202

Fisheries and Oceans | Pêches et Océans

Canada

Canadian Technical Report of
Hydrography and Ocean Sciences 202

1999

Sea State Forecasting in the St. Lawrence River and Gulf

by

Ray Q. Lin[1] and Will Perrie

Ocean Sciences Division
Maritimes Region
Fisheries and Oceans Canada

Bedford Institute of Oceanography
P.O. Box 1006
Dartmouth, Nova Scotia
Canada B2Y 4A2

---

[1]Department of Seakeeping, David Taylor Model Basin
Carderock Division, NSWC
9500 MacArthur Boulevard
West Bethesda, MD 20817-5700

Cat. No. Fs 97-18/202E ISSN: 0711-6764

Correct citation for this publication:

Lin, Ray Q. and Will Perrie. 1999. Sea State Forecasting in the St. Lawrence River and Gulf. Can. Tech. Rep. Hydrogr. Ocean Sci. 202: v + 65p.

Table of Contents

Abstract

Lin, Ray Q. and Will Perrie. 1999. Sea State Forecasting in the St. Lawrence River and Gulf. Can. Tech. Rep. Hydrogr. Ocean Sci. 202: v + 65p.

The entire study involves three phases: (1) development of a best numerical method for wave - current interactions for the St. Lawrence River and Gulf; (2) design and execution of numerical tests for the model; (3) implementation and full validation of the wave - current interaction model with observed and modelled data.

This report marks completion of the second phase of the study. In this phase of the study, we put a new physical term, $\partial c_f N/\partial f$ into the wave - current model. This term is neglected in the standard WAM model. For very large scale motions, especially in deep water, the contributions of the current and varying water depth, as a function of time, may be neglected. However for small scale motions, such as in the St. Lawrence River and Gulf, these contributions and this term become important. For example, the upstream regions of the River are relatively narrow and shallow, with small fetches, except in along river directions. Therefore, the tidal current - wave interactions can become important, becoming very intense under high wind conditions.

For this sort of the study, the semi-implicit scheme, plus a directional filter, as we describe in this report, is appropriate to estimate the wave-current interaction intensity. However, because the filter is very complicated, we apply instead, a third-order Runge-Kutta method, to simplify the problem. The third-order Runge-Kutta method is appropriate for this sort of wave-current interactions problem and for implementation in operational forecast systems for search and rescue in the St. Lawrence River and Gulf.

Résumé

Lin, Ray Q. and Will Perrie. 1999. Sea State Forecasting in the St. Lawrence River and Gulf. Can. Tech. Rep. Hydrogr. Ocean Sci. 202: v + 65p.

L'étude se déroule en trois étapes : (1) développement d'une meilleure méthode numérique pour les interactions vagues-courants dans le Saint-Laurent et le golfe du Saint-Laurent; (2) conception et exécution de tests numériques pour le modèle; (3) mise en œuvre opérationnelle et pleine validation du modèles des interactions vagues-courants à l'aide de données observées et modélisées.

Le rapport marque l'exécution de la seconde étape de l'étude. Lors de cette étape, nous avons introduit dans le modèle vagues-courants un nouveau terme physique, $\partial c_f N/\partial f$, qui est négligé dans le modèle WAM standard. Pour les mouvements de très grande échelle, surtout en eau profonde, on peut négliger les contributions du courant et la différence de profondeur de l'eau, en tant que fonction du temps. Cependant, pour les mouvements de petite échelle, comme dans le fleuve et le golfe Saint-Laurent, ces contributions et donc ce terme deviennent importants. Par exemple, les zones amont du fleuve sont relativement étroites et peu profondes, avec des fetchs limités, sauf dans le sens d'écoulement du fleuve. Par conséquent, les interactions entre le courant de marée et les vagues peuvent devenir importantes, voire intenses par vent fort.

Pour ce genre d'étude, le schéma semi-implicite, assorti d'un filtre directionnel, comme nous le décrivons dans le rapport, est adéquat pour estimer l'intensité des interactions vagues-courants. Cependant, comme le filtre est très complexe, nous appliquons à la place une méthode de Runge-Kutta de troisième ordre pour simplifier le problème. La méthode de Runge-Kutta de troisième ordre convient à ce genre de problème d'interactions vagues-courants et pour la mise en œuvre opérationnelle de systèmes de prévision destinés aux opérations de recherche et sauvetage dans le Saint-Laurent et dans le golfe.

1 Basic Governing Equations

The correct equation for studying the wave - current interactions is an action conservation equation. A detailed discussion of this approach appears in Lin and Huang (1996b) and Lin (1998b).

Both the so-called energy transport equation and the action conservation equation are commonly used in wave modelling. However, according to first principles, wave action is conserved, not the wave energy (Whitham, 1974). Therefore, the action conservation equation is the appropriate equation for studying the wave - current interactions. From the action conservation equation, one can directly calculate the wave - current interactions, in a manner that distinctly separates the calculation, for the analysis and computation of the source functions: the energy input to waves by wind, S_{in}, the energy removed by wave - breaking dissipation, S_{ds}, and the energy transferred and re-distributed within the spectrum by nonlinear interactions, S_{nl}.

By contrast, if one uses a transport energy equation, such as the state-of-art wave model, WAM (see Komen et al: 1994), it becomes very complicated to exactly calculate the wave - current interactions. Therefore, WAM uses a parameterization to calculate the wave - current interactions, as presented by Günther et al (1993). However, these parameterization methods can never give correct solutions in *all* cases (Lin and Huang, 1996b).

2 Nonlinear Dispersion in Wave - Current Interactions

The correct nonlinear dispersion relation for a wave - current interaction study in the St. Lawrence River and Gulf is:

$$\sigma = (gk \tanh kd)[1 + (\frac{9\tanh^4 kd - 10\tanh^2 kd + 9}{8\tanh^4 kd})k^2a^2 + \cdots]^{1/2}. \quad (1)$$

This is fully discussed in Lin and Huang (1996b) and Lin (1998b). By contrast the dispersion relation in WAM or Tolman's WAVEWATCH model is

$$\sigma = gk \tanh kd. \quad (2)$$

Therefore WAM and WAVEWATCH are missing the nonlinear term, which may be very large when the water is shallow.

3 Characteristic Propagation Velocities for Wave - Current Interactions

The correct formulations for characteristic propagation velocities c_θ and c_ω are:

$$\begin{aligned} c_\theta &= \frac{D\theta}{Dt} = \frac{1}{k}\frac{\partial\sigma}{\partial d}\frac{\partial d}{\partial n} + \frac{1}{k}(c_g - c)\frac{\partial k}{\partial n} + \frac{\vec{k}}{k}\cdot\frac{\partial\vec{v}}{\partial n}, \\ c_\omega &= \frac{D\omega}{Dt} = \frac{\partial\sigma}{\partial d}\frac{\partial d}{\partial t} + \vec{k}\cdot\frac{\partial\vec{v}}{\partial t} + \vec{v}\cdot\frac{\partial\vec{k}}{\partial t} + (\vec{v} + \vec{c}_g)\cdot\nabla(\sigma + \vec{k}\cdot\vec{v}). \end{aligned} \quad (3)$$

as discussed in detail in Lin and Huang (1996b) and Lin (1998b).

By contrast, the c_θ and c_ω formulations, as given in the state-of-art WAM wave model are:

$$
\begin{aligned}
c_\theta &= \frac{1}{k}\frac{\partial \sigma}{\partial d}\frac{\partial d}{\partial n} + \frac{\vec{k}}{k}\cdot\frac{\partial \vec{v}}{\partial n}, \\
c_\omega &= 0.
\end{aligned} \tag{4}
$$

By comparison, the c_θ and c_ω by Tolman (1991) are:

$$
\begin{aligned}
c_\theta &= \frac{1}{k}\frac{\partial \sigma}{\partial d}\frac{\partial d}{\partial n} + \vec{k}\cdot\frac{\partial \vec{v}}{\partial n}, \\
c_\omega &= \frac{\partial \sigma}{\partial d}\frac{\partial d}{\partial t} + \vec{k}\cdot\frac{\partial \vec{v}}{\partial t}.
\end{aligned} \tag{5}
$$

The c_θ and c_ω formulations, by WAM or Tolman, are all right only if the normalized wave steepness ($\epsilon = ak\frac{3+\tanh^2 kd}{4\tanh^3 kd}$) is very small. However, in the coastal region or the St. Lawrence River and Gulf, especially where the water is relatively shallow, even when the wave steepness ak is very small, the normalized wave steepness may still be very large. Therefore, WAM and Tolman's WAVEWATCH wave-current interactions will certainly mis-represent the wave - current interactions in the St. Lawrence River and Gulf. Moreover, this is especially true because WAM assumes that $c_\omega = 0$, which therefore makes it insensitive to the wave - current interactions which are effected by the water depth and frequency variation.

In the following discussion, we will show some hypothetical wave - current interaction tests, which will show the difference between WAM and our new formulations. However, it is impossible to make a true comparison between our new formulation and Tolman's WAVEWATCH. This is because Tolman's WAVEWATCH uses unconditionally unstable numerical schemes, which explode in any pure kinematic test. This is shown in in the discussion that follows. Tolman adopts the parameterization term from WAM to represent the wave - current interactions. Therefore, in the sections that follow, we will only compare our new formulations with WAM.

4 WAM Balance Equation and Shoaling/Refraction

Wave - current interactions conserve action (Whitham, 1974). Therefore, to study wave - current interactions we should use the action conservation equation as follows:

$$\frac{\partial A}{\partial t}+\frac{\partial[c_{g\lambda}A]}{\partial\lambda}+\cos^{-1}\phi\frac{\partial[c_{g\phi}A\cos\phi A]}{\partial\phi}+\frac{\partial[c_\theta A]}{\partial\theta}+\frac{\partial[c_\omega A]}{\partial\omega}=S_{ds}+S_{nl}+S_{in}. \quad (6)$$

where A is action energy density, $A = N/\omega$, N is energy density, c_θ and c_ω are given in Equation (3), $c_{g\lambda}$ and $c_{g\phi}$ are as follows:

$$\begin{aligned} c_{g\lambda} &= \frac{c_g\sin\theta+u}{R\cos\phi}, \\ c_{g\phi} &= \frac{c_g\cos\theta+v}{R}. \end{aligned} \quad (7)$$

WAM uses the following energy transport equation:

$$\frac{\partial N}{\partial t}+c_{g\lambda}\frac{\partial N}{\partial\lambda}+c_{g\phi}\frac{\partial N}{\partial\phi}+c_\theta\frac{\partial N}{\partial\theta}=S_{ds}+S_{nl}+S_{in}+refractions.$$

where c_θ and c_ω are given in Equation (4). The refractions are parameterizations which represent the divergent terms in Equation (6).

Having established the analytic expressions for the kinematics, we will present some numerical results to illustrate the differences between the full nonlinear dispersion relation used in our new formulation, as described by Lin and Huang (1996a and 1996b), and Lin (1998a and 1998b) and the linear approximations used in WAM. Of course, in most of the comparisons we cannot totally exclude the influences of the different numerical schemes and different types of model equations. WAM uses the energy transport equation, whereas we use the action conservation equation with a full nonlinear dispersion relationship. We will try to illustrate the effects of nonlinearity and the different types of model equations as far as possible.

5 Numerical Method

To develop an accurate wave model, one not only needs accurate physical source terms, one also needs a numerical method, with minimum dissipation and dispersion, to calculate these physical terms. Unfortunately, WAM uses the classic Euler Scheme, which has huge numerical dissipation and dispersion.

5.1 Euler Scheme

A comparison between the first order Euler scheme, as implemented in WAM, with higher order Euler schemes, in terms of numerical dispersion and dissipation and computational instability, is discussed in this section.

Figure 1 shows the computational instability for the transport equation, using

(a) first order Euler;

(b) second order up-stream (second order Euler);

(c) third order up-stream.

The results show that the first order Euler scheme, as well as its higher order schemes, are all conditionally computationally stable schemes for the transport equation. These are implemented in the WAM model.

To study numerical dissipation and dispersion, we will use a simple test as shown in Figure 2, where 2(a), 2(b), and 2(c) are as in Figure 1. The initial energy density spectral function is given by $N^{(0)} = \exp\{-k[x - (c_g + u)t_o]^2\}$, when k=0.2, t_o =10, and $(c_g + u) = c_1 + c_2[1 = cos(j \triangle x)]$, where c_1=0.6, c_2=0.2, $\triangle x$=0.5, where

(a) Line A represents the true solution,

(b) Line B represents the numerical solution for $\triangle t = 0.25$, and $n = 400$ is the number of time steps,

(c) Line C represents the numerical solution for $\triangle t = 0.5$ and $n = 200$.

Our analysis leads us to following general conclusions:

(i) Simply increasing the order of a numerical scheme will not yield a better solution.

(ii) Although higher-order schemes decrease numerical errors, numerical dissipation and dispersion continue to be excited for any finite order.

(iii) Dissipation dominates when m is odd and dispersion dominates when m is even, where m is the order of the higher-order scheme, $m = 1, 2, 3....$

(iv) When m increases beyond 2, the boundary condition becomes increasingly more complicated.

(v) The key to limiting numerical errors, in any order of Euler upwind scheme, is to use very small $\triangle t$. Unfortunately this requires enormous amounts of computer time.

For studies devoted to wave - current interactions research, there is another more serious shortcoming to the Euler upwind schemes: we have to deal with problems which have finite spectral bandwidth. In the finite bandwidth problem, dissipation and dispersion will be nonuniform for different wave components. Such effects are impossible to separate from other real physical processes, which are expressed in the various source functions, wind input S_{in}, dissipation, S_{ds} and nonlinear interaction, S_{nl}, which are all wavenumber and frequency dependent.

5.2 Numerical Schemes for Transport and Conservation Equations

The first order Euler scheme, higher order upwind schemes, leap-frog scheme, ICN scheme, SHASTA scheme, etc. are appropriate for the transport equation, but not appropriate for the action conservation equation. This is relevant for the wave - current interaction problem because the first order Euler scheme, higher order upwind schemes, leap-frog scheme, ICN scheme, SHASTA scheme, etc. are all conditionally stable for the transport equation. However all these schemes are unconditionally unstable for the conservation equation. The problem is that the Gibbs instability will be generated when these schemes are applied to the conservation equation, and the solution will grow with time, without bound. Alternately, oscillations will be generated in the numerical solutions, that will never converge, with time. See Phillips (1959).

Figures 3a-c show instabilities for these numerical schemes for the transport equation. Figures 4a-c, show corresponding effects for the conservation equation. These results are for the following schemes:

(a) second-order upwind scheme;

(b) third order upwind scheme;

(c) ICN scheme.

where

(i) Line A represents the true solution,

(ii) Line B represents the numerical solution for $\triangle t = 0.1$, for time step $n = 1000$,

(iii) Line C represents the numerical solution for $\triangle t$=0.05 for time step, n=2000,

(iv) Line D represents the numerical solution for $\triangle t$=0.0125 for time step, $n = 8000$.

From Figures 3a-c, we see that the higher order upwind schemes are stable (numerical solution less than 1). However, the ICN scheme is unstable, because its numerical solutions are greater than 2. If the time step is smaller than what is displayed in these calculations, the numerical solutions of the ICN scheme can be less than 1, implying that it is stable. This is not shown in Figures 3a-c of this report. See Lin and Huang (1996b).

However, Figures 4a-c, for the conservation equation, show that all the numerical schemes are highly unstable. Figure 4a shows that

(a) the numerical solutions of the second order up-stream scheme become greater than 1;

(b) numerical solutions of the third order upwind scheme are more unstable, becoming greater than 2;

(c) the ICN scheme becomes greater than 25×10^{15}, implying that ICN is the most unstable scheme.

These schemes are unconditionally unstable for the conservation equation because $\partial_x(c_{gx} + u) \neq 0$. This statement can be found in many fundamental textbooks such as Kreiss and Lorenz (1990), Shu and Osher (1989), Osher (1993), as well as Book et al (1975). Moreover, even more than two decades ago, in the 1970s, when Book and his colleagues solved the conservation equation, Gibbs instability was the major problem which confronted them. It is still unresolved.

If the numerical scheme is unconditionally unstable, then its numerical errors can't be reduced by adopting second or higher order schemes. In fact there are many cases which show that second or higher order schemes may increase the instabilities. For example, the second-order Euler scheme in the conservation equation is much more unstable than the first-order Euler scheme. Please see Figure 4a, which shows the second-order Euler scheme for

the conservation equation. The second-order Euler scheme totally explodes, whereas under the same conditions, the first-order Euler is much more benign. In fact it is relatively well behaved.

The SHASTA scheme is an ICN-type scheme, with artificial diffusion added, which is called Flux Corrected Transport, or FCT, (Boris and Book, 1973, 1975, and 1976; Book et al, 1975; Book and Zalesak, 1981; Book, 1993). Both schemes have similar mathematical characteristics, are unconditionally unstable, and exhibit a large tail with negative energy (Book et al, 1975; Book and Zalesak, 1981). FCT cannot change the intrinsic characteristics of the numerical schemes. If a numerical method is unconditionally unstable, then adding diffusion cannot completely eliminate instabilities. Furthermore, real solutions are contaminated when artificial diffusion is numerically added to dampen unstable modes. Therefore, from a mathematical point view, adding diffusion can't be considered as introducing a different scheme. Moreover, because FCT itself is computationally unstable (Book, 1993), it may cause SHASTA to explode faster than the corresponding ICN scheme. Therefore, we suggest that it is not necessary to discuss this class of numerical schemes.

5.3 Implicit Scheme for Action Conservation Equation

We propose a second order semi-implicit scheme with a directional filter for the action conservation equation. The semi-implicit scheme is given by the following equations:

$$\mathbf{A}_j^{n+1} - \mathbf{A}_j^n = \frac{1}{2}[(\mathbf{F}_{j-1}^{n+1} - \mathbf{F}_j^{n+1}) + (\mathbf{F}_{j-1}^n - \mathbf{F}_j^n)]. \tag{8}$$

The stability parameter is

$$\Lambda = \frac{(1-a) - ib}{(1+a) + ib},$$

$$|\Lambda|^2 = \frac{(1-a)^2 + b^2}{(1+a)^2 + b^2}, \tag{9}$$

where

$$a = \frac{\mu_j}{2} - \frac{\mu_{j-1}}{2} \cos k \triangle x,$$

and

$$b = \frac{\mu_{j-1}}{2} \sin k \triangle x.$$

The dispersion parameter is

$$-\theta^* = tan^{-1} \frac{b}{(1-a)} \overset{k\triangle x \to 0}{\longrightarrow} \mu k \triangle x.$$

Therefore,

$$(c_g + u)^* = \frac{-\theta^*}{k \triangle t} \overset{k\triangle x \to 0}{\longrightarrow} c_g + u. \tag{10}$$

From Eq. (9), one can see that second-order semi-implicit schemes are stable when $a \geq 0$, and when $\mu \leq 0.5$, $100\% \geq |\Lambda| \geq 90\%$. Therefore, computational dissipation is very small and does not vary significantly with μ, when $\mu \leq 0.5$. However, Eq. (10) indicates that this scheme is dispersive and non-conservative when $k \triangle x \neq 0$.

Unlike the ICN scheme, the dispersion in this scheme will not generate a sign changing tail. However, it will spread action around the propagation direction and cause the total action to increase. Non-conservation of action is a classical difficulty encountered in numerical solutions of hyperbolic conservation equations. To compensate for the non-conservative property, we introduce a directional filter to maintain conservation of action. The filter forces total action to be conserved and suppresses numerical dispersion by a weighting function. This filter is not related to $\triangle t$, $\triangle x$, $(c_g + u)$, or μ. A more detailed description is given in the Appendix.

Figure 5 shows the distribution of **N** for the new scheme. This is in the same format as Figure 4, except that it is for the second-order semi-implicit scheme, with $\triangle t$ =1.0, 0.5, and 0.125, which are ten times greater than the $\triangle t$ in Figure 3. Figure 5 is based on Equation (8) with the directional filter. Figure 5 shows that numerical simulations are computationally stable. The maximum values equal about 83% of the true solutions when $t = 100$. The total energy remains the same, and the results do not vary significantly with $\triangle t$, $\triangle x$, and $c_g + u$, when μ is less than unity.

If one considers the direction filter difficult to use, one may apply the third-order Runge-Kutta method. The accuracy of the latter method may be only slightly lower than that of our implicit scheme+direction filter method. Moreover, the CPU time may require only a little more time than our implicit scheme+direction filter method. However, this is a computationally stable scheme, and it is easy to use. If the Equation (6) can be simplified as,

$$\frac{\partial A}{\partial t} = N(A, \vec{K}, x, y, t, h),$$

where $N(A, \vec{K}, x, y, t, h)$ is flux terms, then third-order Runge-Kutta method is

$$\begin{aligned} y_1 &= (dt/2)N(A^{(n)}, \vec{K}, x, y, t, h); \\ y_2 &= (3dt/4)N(y_1, \vec{K}, x, y, t, h); \\ A^{(n+1)} &= (dt/9)[2N(A^{(n)}, \vec{K}, x, y, t, h) + 3N(y_1, \vec{K}, x, y, t, h) + 4N(y_2, \vec{K}, x, y, t, h)]. \end{aligned} \tag{11}$$

5.4 Comparison of our Implicit Scheme with WAM Scheme

In this section, we report results of comparisons between our new semi-implicit scheme, with direction filter, with competing schemes. We consider the first-order Euler upwind scheme in WAM and the ICN scheme in Tolman (1992)'s WAVEWATCH, as implemented at NCEP in Washington.

From the point of view of numerical analysis, the WAM model uses the transport equation. Therefore, the first order Euler scheme, as implemented for WAM, will be conditionally computationally stable, although it will experience rapid damping, as shown in Figure 2a. In fact, it is possible that a reduction to 70-80% of the true solution will occur due to damping, in a single time step (Lin and Huang, 1996a).

WAVEWATCH by Tolman (1992) used a ICN scheme, implemented for an action conservation equation. Therefore, the resultant scheme is unconditionally computationally unstable, as Tolman described in his 1992 paper. He tried to use the source functions, S_{in}, S_{ds} and S_{nl}, to prevent the computational instability, by using a parameter to reduce the divergent term, in the conservation equation. Thus, only when the source functions dominate does the solution not explode. This is shown in Figure 4c. The ICN scheme is the most poor numerical scheme, of all candidate schemes, for the conservation equation. In contrast, our new semi-implicit scheme, with the directional filter, as shown in Figure 5, as implemented for the action conservation equation, is unconditionally computationally stable. Furthermore, the semi-implicit scheme is *not* sensitive to the time step, group velocity or the current. These are important characteristics for a wave - current interaction study.

5.5 Stability

Developing a numerical scheme to study the wave - current interactions involves standard criteria, such as:

(a) The numerical scheme must be at least conditionally stable, which is the most important principle. If a numerical method doesn't satisfy this principle, the scheme is not valid;

(b) The dissipation and dispersion should be as small as possible;

(c) The model should be computationally efficient.

The most important overall principle, in developing a numerical scheme, are computational stability conditions. Since WAM uses a transport equation, the usual the numerical schemes, such as the Euler upwind scheme, the leap-frog scheme, the ICN scheme, SHASTA, etc. are all conditionally stable. One only needs to find the conditions for computational

stability, and then restrict computations so that they remain within the computational stable area. Then the computational instabilities will not occur. The problem with the WAM model is not that of computational instability. The problem is that the basic equation is the energy transport equation, with a parameterization for refraction. Thus some wave - current interactions are missed in some situations. Alternately, and of equal as importance, these terms are misrepresented and this results in biased simulations.

A competing numerical scheme is that of Tolman (1992), using the action conservation equation. He applied these standard numerical schemes to solve his conservation equation. Therefore, his results are guaranteed to explode, especially since he used the most unstable schemes, namely the ICN scheme. Tolman (1992) claims that SHASTA, and similar other schemes, such as his ULTIMATE-QUICKEST scheme, have now improved his ICN scheme. However, according to the above discussion, so long as these numerical schemes are based on an unconditional unstable scheme, they must eventually explode, as shown in Figure 4c. The WAM model did not have this problem.

6 Hypothetical Tests:

In a river estuary, such as the St. Lawrence River and Gulf, we want to see wave - current interactions, effectively defining the variations of the sea state, due to effects of bottom topography and time varying tidal currents. To eliminate other complications, the tests are designed to study the propagation of waves over a very wide uniform River. Therefore, these tests are conducted in an idealized up-stream and down-stream region with bottom topography which is somewhat similar with the St. Lawrence River.

6.1 Tests with No Tide

In this section, we investigate only the effect of bottom topography on wave propagation. To avoid the boundary effects, we assume a very wide river. We consider a 300 km length of the river, and open boundaries for both sides of the river. We assume the depth changes from 2995 m in the extreme down-stream boundary of this "river", to 2.5 m at the extreme up-stream boundary. We assume the river flows from west to east. In all the tests, the sea state is represented by a continuous and steady swell system, given by the spectrum shown in Figure 6(a). The corresponding energy propagation direction is labelled by a numbering system used in the computer, as indicated in Figure 6(b). The swell spectrum is prescribed at every grid point at the open ocean boundary (the deep water down-stream boundary of this hypothetical wide river).

For tests reported here, we assume the incoming swell system has relatively small angular and frequency distribution ranges, with the maximum energy density propagating in direction number 6. For each test, the test area is assumed to be calm initially. The swell system is assumed to enter the test region from the open ocean side (at the down-stream boundary) and propagate upstream towards shallower water. To allow for the dissipation of transients, during which the highest frequency components pass from the system, the models are run for five days before test results are selected for detailed comparisons. All the computations for our new formulation (Lin and Huang, 1996a and 1996b) are performed in terms of action density, as given in the model action conservation equation. However, the results are presented in terms of the energy density spectrum, because buoys measure energy density and it is the "standard" traditional variable used in comparisons.

For the assumed "river", the grid mesh size consists of $\triangle x = \triangle y = 12.5\ km$, $\triangle\theta = \pi/6$, and $\triangle f = 0.1f$. The time step of the WAM is 5 min (*minutes*). By comparison, the time step of our new formulation (Lin and Huang, 1996a and 1996b) is 10 min.

Because we use the full nonlinear dispersion relationship, which we

derived based on perturbation analysis, its ordering and magnitude are all energy density related. Therefore, we have to always verify that, as the water depth decreases, the increasing energy density does not cause the higher order terms to overpower the lower order ones. To guarantee this ordering, we impose a breaking criterion. We demand that the waves will break when $ak \geq 0.4$ in the computations. When this limit is exceeded, we set the wave energy to zero. This criterion is rather conservative. By comparison, the Stokes limit puts ak very close to unity. In view of the available laboratory and field observations, as summarized by Huang et al. (1986), we feel that this choice is justifiable. In future tests, other values can be easily substituted, if they are proven to be more realistic.

6.2 Tests with Varying Depth but No Current

In this section, we present the response of our new formulations (Lin and Huang, 1996a and 1996b), in comparison with the WAM wave model. This is in the case when there is no current but the depth varies from very deep to very shallow.

This is the simplest test condition. The results can serve as a reference benchmark which will be relevant for the results we obtain when we examine the variations of more complicated conditions. We will run the WAM model for this case only. The results would be identical for all the subsequent WAM cases with various currents, because the WAM version we have access to does not include the wave-current interactions or depth change as part of the model. Therefore for the comparisons with the subsequent cases between our new formulation and WAM, we can only refer to the WAM results of this case.

Figures 7a-c shows the numerical simulation of energy density spectrum by the WAM model: Figure 7a represents the energy density in the direction number 4, towards the up-stream direction. Figure 7b represents the energy density in the direction number 5. Figure 7c represents the energy density in the direction number 6. In all these figures, the horizontal axis represents the downstream-to-upstream physical distance, starting from the

open ocean end of our assumed hypothetical "river". The vertical axis of these figures represents the logarithm of frequency.

Our new model results are shown in Figures 8a-c. As expected, Figures 8a-c show that the swell energy at any frequency remains constant along the propagation path. This is a consequence of energy transport without sources or sinks. These represent the current state-of-the-art wave model results. Since the WAM does not include current effects, the WAM results, with assumed currents, will be identical to those WAM results presented here in Figures 7a-c.

As a special test of the effects of different model equations (energy transport equation *or* action conservation equation), our new formulation (Lin and Huang, 1996a and 1996b) is used here with the linear dispersion relation as implemented in WAM. Even with this simplification, the depth effects still become dominating. Energy pile-up occurs, as shown in the Figures 8a-c, as predicted by the analytic results of Phillips (1977). Other than this expected energy pile-up, there is an unexpected shift of energy toward lower frequencies near the up-stream boundary (where the water is shallow), in the energy propagation directions number 5 and 6. The results from WAVEWATCH by Tolman is showed in Figure 9(a) for direction number 4, and Figure 9(b) for number 5 direction. Based on our earlier discussions of Tolman's WAVEWATCH model, it is not a surprise that the model results explode even without current.

6.3 Frequency Downshifting

In this section we consider frequency downshifting in situations where waves interact with currents and depth varies from deep to shallow, as in the hypothetical "river" example described above. We use our (correct) nonlinear dispersion with characteristic propagation velocities, in comparison with results from the WAM model.

The frequency shift can be explained by the second term of Equation (3). For the cases with no current, or steady state current when $\vec{k} \cdot \vec{v} = 0$, c_ω

depends only on:

$$(\vec{c}_g + \vec{v}) \cdot \bigtriangledown\sigma = \frac{\partial\sigma}{\partial d}(\vec{c}_g + \vec{v}) \cdot \bigtriangledown d.$$

We note that,

$$\frac{\partial\sigma}{\partial d} = \frac{g[ksech(kd)]^2}{2\sigma} > 0;$$

which implies that the sign of c_ω depends on $(\vec{c}_g + \vec{v}) \cdot \bigtriangledown d$. Therefore, when waves propagate into shallow water, it follows that c_w must become negative. The negative sign here contributes to the downshift of frequency. By contrast, it should be noted that this term is not included in the WAM. This is therefore one reason why WAM cannot fully model coastal regions or similar regions, such as the St. Lawrence River and Gulf.

6.4 Tests with a Hypothetical Periodic Tidal Current

In this section, we present hypothetical tests using computer-generated data. These tests investigate wave-current interactions for coastal topographic geometries which have some similarity with the geometries of the St. Lawrence River and Gulf. This includes similar current speeds, similar topographic bottom slope, for reasonable wave spectra.

Specifically, we consider the hypothetical "river", described in Section 6.1, and we add a 24 hour periodic tidal current, propagating along the St. Lawrence River. The tidal current increases from 0.2 m/s at the deep-water downstream computational "boundary" of the river to 1 m/s at the shallow-water upstream computational boundary. In this case, we have a time-dependent current as well as topographic features. Therefore, we will present more detailed comparisons between our new wave - current interaction model with linear and nonlinear dispersion relationships, than were presented in Section 6.1. As yet we do not model the effects of side boundaries, as they occur in the St. Lawrence River and Gulf.

Figures 10a-c show the results from the numerical simulation for the energy spectrum distribution in our new wave - current interaction model. In these results, we assume a linear dispersion relationship for the direction

numbers 4, 5 and 6 respectively (specified in Figure 6b). Figures 11a-c show the corresponding results when a nonlinear dispersion relationship is used. Because the breaking criterion was only imposed on the nonlinear dispersion case, it follows that the effects of breaking show up only in the nonlinear cases.

The effects of currents in these cases are drastic, as listed below:

(a) The energy density fluctuates with the period of the tidal current. As shown in Figure 10a, the maximum energy density values at the upstream computational "boundary" vary from 1.6 m^2/Hz to 2.3 m^2/Hz, depending on the tidal cycle.

(b) Moreover, in both Figures 10a and 10b, the locations of the maximum values move with the tidal cycle.

(c) However, in Figure 10c, the maximum energy density regions always stay in the deep ocean (closer to the downstream computational "boundary") and only extend their fronts with the tidal cycle.

Comparisons were made of the cases with linear and nonlinear kinematics. We found that the main nonlinear effect is to eliminate the energy pile up at the upstream compuational "boundary", which was previously experienced in Figures 8a-c. This is more a consequence of the imposed breaking criterion than to the dispersion relationship. The lack of breaking is also the main reason why the linear model shows more total wave energy than the nonlinear model.

Nonlinear effects, as expected, should be weak at the open ocean boundary (the downstream computational "boundary" for this hypothetical river). This is what the results indeed show. In relative terms, the wave-current interactions should be stronger near shallow water upstream computational "boundary". Unfortunately, the breaking criterion has clouded this issue. A weakening of the effect can, however, be discerned in these figures. The nonlinear dispersion does cause more energy to get closer to, but not at, the upstream computational "boundary", as shown in Figures 10c versus

7c. However, this is only a relative term. Other studies should be devised to clarify these effects.

6.5 Significant Wave Height in the New Wave Model

In this section, we will show the new wave - current interaction model results in an ideal St. Lawrence River. These results include the real wave-current interactions, as well as the effect of currents and water depth, which vary with time, and also the standard WAM source function terms, namely S_{in}, S_{nl}, and S_{ds}. In the following tests, we assume a maximum wind speed of 17m/s which blows constantly for 24 hours. This is to demonstrate, even in extremely windy cases, comparatively speaking, that the new physical terms and real wave-current interactions still strongly affect the solutions. Since the S_{nl} is calculated by DIA (the discrete interaction approximation), and therefore highly inaccurate, implying high inaccuracies in the two-dimensional energy spectrum, we only show the significant wave height H_s. Inaccuracies in the DIA formulation for S_{nl} are discussed in Lin and Perrie (1999).

We assume that the River can be idealized as being along the x-coordinate axis from up-stream ($x = 0$) to down-stream ($x = 1000km$). In these tests the space discretization is $5km$ and the time-step is $5seconds$. The width of the river is $20km$ at the upstream "end" of the grid, and $100km$ at the down-stream "end", the mouth of the St. Lawrence River. The width of the River is assumed to linearly decrease from down-stream to up-stream. The length of the St. Lawrence River is assumed to be $1000km$. The water depth is assumed to fit the function:

$$h = -300 * \exp(i - 1000km)^2/294000,$$

implying that water depth decreases exponentially from down-stream to up-stream. The tidal current is assumed to fit the form $0.4\sin(2\pi t/T)$, where t is time, and T is the period of the tide and equal to $24hours$. The river current due to the gravity force, from up-stream to down-stream, is assumed to have a maximum of $1m/s$. Both the tidal current and the gravity forced

current are proportional to the bottom steepness, *in actuality.*

Figure 12a shows the significant wave height H_s distribution at 6-hourly intervals for a one day period when the wind speed of $17m/s$ blows constantly along the y dimension, which is perpendicular to the assumed length of the river, along the x-axis. The model has had $24hours$ to warm up, prior to achieving the results shown in Figure 12a. In this case, the river bottom is assumed completely smooth, with no bottom elevation, no "bumps". The H_s contours are at intervals of *one meter.* We can see that H_s increases along the wind direction. The maximum H_s is near the North end of the River mouth, because that is where the river is widest and the waves have the longest fetch, when the wind direction is across the river length. Corresponding results may also be obtained from the WAM model, as shown in Fig. 12b, where H_s has a maximum value of 6.1m.

The most interesting phenomena, which are not predicted by the WAM model, are related to the tidal current and water depth variability. These two effects cause the maximum H_s to have a daily movement along the x coordinate, which is the direction along which the assumed river flows. The maximum H_s itself also oscillates periodically in time. This is very important for simulating and predicting H_s on the river. Moreover, because WAM indirectly calculates wave-current interactions, using parameterizations for refraction and reflection, and also uses a strong numerical dissipation and dispersion method, there may be some differences between WAM and between a new wave -current interaction model, which does not have these features. The numerical method is discussed more in the Appendix.

Figure 13a is the same as Figure 12a, except the wind is blowing along the river length from up-stream to down-stream direction. In this case, the maximum H_s appears in the down-stream region. However, due to the wave-current interactions, the maximum H_s does not converge to the most extreme downstream region of the gird. Moreover, this maximum oscillates in both space and time. The difference can be $2m$ height, between the maximum and minimum oscillations. The $4m$ isoline is indicated in Figures 13a-b, as it goes through its cyclic oscillation. Corresponding results from WAM are presented in Figure 13b, showing non-oscillatory H_s contours as in Figure 12b.

Figure 14a is the same as Figure 13a, except the wind is blowing along the river from down-stream to up-stream. In this case, the maximum H_s is located near the up-stream region of the grid (in the down-wind direction). However, as in Figure 13a, the maximum H_s does not converge to the extreme up-stream portion of the grid. As in Figure 13a, because of the wave-current interactions H_s, oscillates in space and in time. Corresponding results from WAM are presented in Figure 14b, showing non-oscillatory H_s contours, as in Figures 12b and 13b.

Figure 15a is an ideal bump near the river mouth. We assume the river is uniformly $100km$ wide and $300m$ deep, whereas the bump is $12km$ wide, $200m$ high, and $100m$ below the sea surface. Figure 15b is the same as Figures 12a-b, except that there is no wind, and the bottom topography near the river mouth is described in Figure 15a. The bump is in the centre of the figure. The tidal current is periodal, as discussed above. We assume that the right side is downstream and the left side is upstream. These are swell waves. We can see that the maximum significant wave height H_s oscillates on top of the bump. This "bottom-forced" wave is sometimes very significant. See Pedlosky (1979). Its magnitude depends on the free wave frequency (Burger number, $B = Nh/f_C W$, where N is the buoyancy force, W is the width of the bump, h is the height of the bump. If f_C, the Coriolis force, is close to the forcing frequency, for example the tidal current, resonance can occur. The significant height H_s will increase very significantly on top of the bump. To predict this phenomenon we need the new physical term presented in this study and in Lin and Huang (1996b). This term is not in WAM. Corresponding results for WAM are given in Figure 15c. This shows no contours indicating that swell waves in WAM do not feel the bottom. In this case 5.2m waves simply propagate through the space-grid of the model.

7 Summary

Based on our comparisons, we conclude that our new wave - current interaction model will produce more realistic results than the WAM model, due to improved numerics and kinematics. We note that even for the case of a

flat bottom of finite depth, the numerical dispersion and the dissipation in WAM will annihilate energy, computationally. This is discussed in Section 5. Additional differences between the two models become obvious whenever there are ambient currents and depth changes.

In the neighbourhood of up-stream computational "boundary", for the hypothetical river presented in this report, tidal currents and depth changes are the norm rather than the exception. Therefore, any model that is to be applied to these up-stream regions should definitely include the ability to simulate ambient currents and depth changes. Our new wave - current interaction model is based on the action conservation law. This enables us to readily include the current effects. Our model also includes a detailed computation of the dispersion effects due to unsteady current and bottom topography. This is achieved because our new model includes the new physical term, $\frac{\partial[c_f A]}{\partial f}$. This term includes the variation of current and water depth, with time. This term is not imporatnt for large scale motions and deep water. It becomes important when the water is shallow, and small scale, like wave prediction on the St Lawrence River and Gulf.

From the model results, we have shown that there are significant differences between the WAM wave model and our new wave - current interaction model, especially when there is a steady or unsteady current, or when a rough bottom topography and shallow waters are included. Comparison with the analytic results of simpler cases (as given decades ago by Phillips, 1977) convinces us that the new model represents the kinematics more realistically, than contemporary state-of-the-art models, such as WAM. Based on our studies here, we conclude that our new wave -current interaction model offers a better simulation of the St. Lawrence River and Gulf, than the WAM wave model.

8 Appendix

The directional filter is adopted to maintain the total action conservation. In a numerical solution of a differential equation in a multidimensional domain, it is necessary to take turns simulating each dimension while keeping the other dimensions frozen for the A-grid distribution, except in the Essentially Non-Oscillatory Shock-Capturing Scheme, (ENO) (Shu and Osher, 1989). The directional filter introduced here serves exactly this purpose, as in the ENO method, although the directional filter is designed for multi-dimensional problems. The details of the directional filter will be discussed in a separate paper. We will offer the following outline to explain the essential features and the design principles of this filter. In a conservation equation of the type given by Eq. (6), we assume that the original total action, $TA^{(n)}$ is expressed as

$$TA^{(n)} = \sum_{j=1}^{L} A_j^{(n)},$$

in which n represents the time step, j represents the grid point number, and L is total number of grids. After m time steps, the total energy will be

$$TA^{(n+m)} = \sum_{j=1}^{L} A_j^{(n+m)}.$$

If the action energy at each grid is conserved after m time integrations, then we will have the following equation:

$$Filter_j^{(n+m)}(A_j^{(n+m)} - FF_j^{(n+m/2)} \triangle t) = A_j^{(n)}, \tag{A.1}$$

in which

$$FF_j^{(n+m/2)} = - \bigtriangledown \cdot (\vec{c}_g + \vec{u})_j^{(n+m/2)} A_j^{(n+m/2)} + forcing_j^{(n+m/2)},$$

where forcing represents the source functions which are assumed to be zero here. Eq. (A.1) can be rewritten for total action as

$$\sum_{j=1}^{L} \log_{10} Filter_j^{(n+m)} + \sum_{j=1}^{L} \log_{10}(A_j^{(n+m)} - FF_j^{(n+m/2)} \triangle t) = \sum_{j=1}^{L} \log_{10} A_j^{(n)}. \tag{A.2}$$

We assume the $Filter_j^{(n+m)}$ to be a highly directional function, in terms of $\cos^2 \alpha_j$; and we define the filter as

$$Filter_j^{(n+m)} = [\cos^2 \alpha_j]^{rr^{(n+m)}}, \qquad when \qquad \cos \alpha_j > 0,$$

$$Filter_j^{(n+m)} = 0, \qquad when \qquad \cos \alpha_j \leq 0, \quad \text{(A.3)}$$

where α_j is the angle between the the grid j and the grid jm, and $\alpha_j = 2\pi(j-jm)/l$ (with jm indicating the grid where maximum value occurs, and l is a function of the width of the energy spectrum). If the action spectrum $A_j^{(n+m)}$ has more than one maximum, we should define jm_1, jm_2,... and l_1, l_2,... corresponding to each local action maximum. Combining Eq. (A.3) with (A.2), we have

$$rr^{(n+m)} \sum_{j=1}^{L} log_{10}(\cos^2 \alpha_j) = \sum_{j=1}^{L} \log_{10} A_j^{(n)} - \log_{10}[A_j^{(n+m)} - FF_j^{(n+m/2)} \triangle t]; \quad \text{(A.4)}$$

and consequently,

$$rr^{(n+m)} = \frac{\sum_{j=1}^{L} \log_{10} A_j^{(n)} - \sum_{j=1}^{L} \log_{10}[A_j^{(n+m)} - FF_j^{(n+m/2)} \triangle t]}{\sum_{j=1}^{L} \log_{10} \cos^2 \alpha_j}. \quad \text{(A.5)}$$

The accuracy of the energy conservation can be defined as high as one wants. This filter is very effective for the second-order semi-implicit scheme, which was introduced here, in the Appendix of this report. With this filter, the numerical scheme is computationally stable, and the dispersion effects are largely eliminated. This filter can produce reasonable numerical solutions as shown in Figures 5, 10 and 11.

9 Acknowledgements

This wave-current study was funded by the Coast Guard (Canada) Search and Rescue New Initiatives Fund (SAR-NIF). The wave modelling program at BIO is funded by the Federal Panel on Energy Research and Development (Canada) under Project No. 534201.

References

[1] Book, D. L., J. P. Boris, and K. Hain, 1975: Flux-corrected transport. II: Generalization of the method. *J. Comput. Phys.*, Vol. 18, 248-283.

[2] Book, D. L. and S. T. Zalesak, 1981: Flux-corrected transport. *Finite-Difference Techniques for Vectorized Fluid Dynamics.* D. L. Book, Ed., Springer, 29-55.

[3] Boris, J. P., and D. L. Book, 1973: Flux-corrected transport I. SHASTA, a fluid transport algorithm that works. *J. Comput. Phys.*, Vol. 11, 38-69.

[4] Boris, J. P., and D. L. Book, 1975: Solution of the continuity equation by the method of flux corrected transport. *Methods Comput. Phys.*, Vol. 16, 85-129.

[5] Boris, J. P., and D. L. Book, 1976: Flux-corrected transport III. Minimal error FCT algorithms, *J. Comput. Phys.*, Vol. 20, 397-431.

[6] D. L. Book, 1993, private communication.

[7] Günther, H., Hasselmann, S., P.A.E.M. Janssen, 1993: The WAM model cycle4. DKRZ WAM Model Documentation.

[8] Huang, N. E., L. F. Bliven, S. R. Long, and C. C. Tung, 1986: An analytic model for oceanic whitecap coverage. *J. Phys. Oceanogr., 16,* 1597-1604.

[9] Komen, G. J., L. Cavaleri, M. Donelan, K. Hasselmann, and P. A. E. M. Janssen, 1994: *Dynamics and Modelling of Ocean Waves* Cambridge University Press, Cambridge, 512pp.

[10] Kreiss, H. O. and J. Lorenz, 1990: *Initial Boundary Value Problems and Navier-Stokes Equation.*, Cambridge press.

[11] Lin, R. Q. and N. H. Huang, 1996a:The Goddard Coastal Wave Model. Part I: Numerical Method. *J. of Phys. Ocean.* Vol. 26, No. 6, 833-847.

[12] Lin, R. Q. and N. E. Huang, 1996b: The Goddard Coastal Wave Model. Part II: Kinematics. *J. of Phys. Ocean.* Vol. 26, No. 6, 848-862.

[13] Lin, R. Q., 1998a: Reply to comments on Part1 by Tolman et al. In Press in JPO.

[14] Lin, R. Q., 1998b: Reply to Comments on Part II by Tolman et al. In Press in JPO.

[15] Osher, S., 1993, private communication.

[16] Pedlosky, J., 1979, Geophysical Fluid Dynamics, *Springer-Verlag*, 624pp.

[17] Phillips, N. A., 1959: An example of non-linear computational instability, in "Atmosphere and Sea in Motion," Rossby Memorial Volume (B. Bolin, Ed.) P. 501. Rockefeller Institute Press, New York.

[18] Phillips, O. M., 1977: The dynamics of upper ocean, Cambridge University Express. The Second Edition, 235pp.

[19] Shu, C. W. and S. Osher 1989: Efficient implementation of essentially non-oscillatory shock-capturing scheme, II *J. Comp. Phys.* Vol. 83, 32-78.

[20] Tolman, H. L., 1991: A third-generation model for wind waves on slowly varying, unsteady, and inhomogeneous depth and currents. *J. Phys. Ocean.* Vol. 21, 782-797.

[21] Tolman, H. L., 1992: Effects of numerics on the physics in a third-generation wind-wave model. *J. Phys. Ocean.*, Vol. 22, 1095-1111.

[22] Whitham, G. B., 1974: *Linear and Nonlinear Waves.* John Willey, New York, 628pp.

Figure Captions

Figure 1. Computational instabilities for the transport equation: with (a), first order Euler scheme; (b) the second-order up-stream scheme, (c), the third-order up-wind scheme.

Figure 2 A simple test for numerical dissipation and dispersion for the transport equation.

Figure 3 A simple test for computational instabilities, numerical dissipation and dispersion for the transport equation, (a) the second-order up-wind scheme, (b) the third-order up-wind scheme, and (c) the ICN scheme (α=0.).

Figure 4 A simple test for computational instabilities, numerical dissipation and dispersion for the conservational equation, (a) the second-order up-wind scheme, (b) the third-order up-wind scheme, and (c) the ICN scheme (α=0.).

Figure 5 A simple test of a semi-implicit scheme + directional filter for computational instabilities, numerical dissipation, and numerical dispersion for conservation equation.

Figure 6 (a) The directional energy spectrum of a swell system used in the propagation test. (b) the energy propagation direction labeled by a number system used in the computation.

Figure 7 Numerical results of WAM, which show that the swell in Figure 6 propagates along the St. Lawrence River, (a) angle number = 4; ((b) angle number = 5; (c) angle number = 6.

Figure 8 Numerical results of our new wave-current interaction model showing that the swell in Figure 6 propagates along the St. Lawrence River without current, (a) angle number = 4; ((b) angle number = 5; (c) angle number = 6.

Figure 9 Numerical results for Tolman's WAVEWATCH model, showing that the swell in Figure 6 propagates along the St. Lawrence River without current, (a) angle number = 4; ((b) angle number = 5.

Figure 10 Numerical results for our new wave-current interaction model with linear dispersion, showing that the swell in Figure 6 propagates along St. Lawrence River with tidal current, (a) angle number = 4; (b) angle number =5, (c) angle number = 6.

Figure 11 As in Figure 10, numerical results for our new wave-current interaction model, assuming nonlinear dispersion.

Figure 12. (a) Significant wave height H_s distribution for an idealized St. Lawrence River, with smooth bottom topography and wind speed $17m/s$ oriented perpendicular to the central axis of the river, and with an assumed tidal current of $0.4m/s$ with a $24hour$ period. (b) From WAM model.

Figure 13. (a) As in Figure 12a, except the wind is oriented along the river, from down-stream to up-stream. (b) From WAM model.

Figure 14. (a) As in Figure 12a, except the wind is oriented along the river, from up-stream to down-stream. (b) From WAM model.

Figure 15. As in Figure 12a, except no wind, and there is a bottom bump near the river month: (a) the ideal bump, (b) isolines for significant wave height as a function of time in minutes, (c) isolines for WAM model.

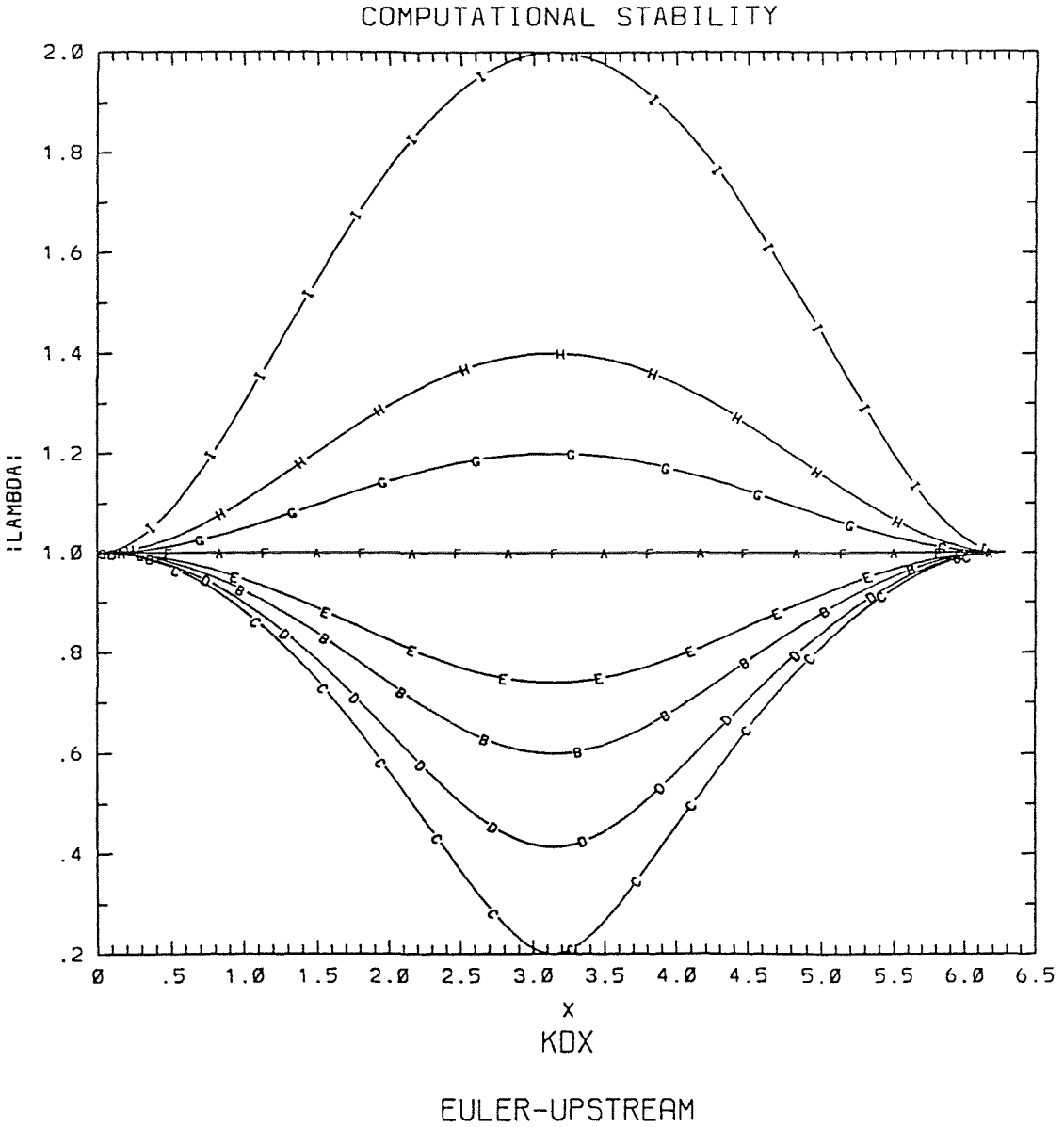
COMPUTATIONAL STABILITY
2.0
1.8
1.6
1.4
1.2
1.0
.8
.6
.4
.2
|LAMBDA|
0
.5
1.0
1.5
2.0
2.5
3.0
3.5
4.0
4.5
5.0
5.5
6.0
6.5
X
KDX
EULER-UPSTREAM

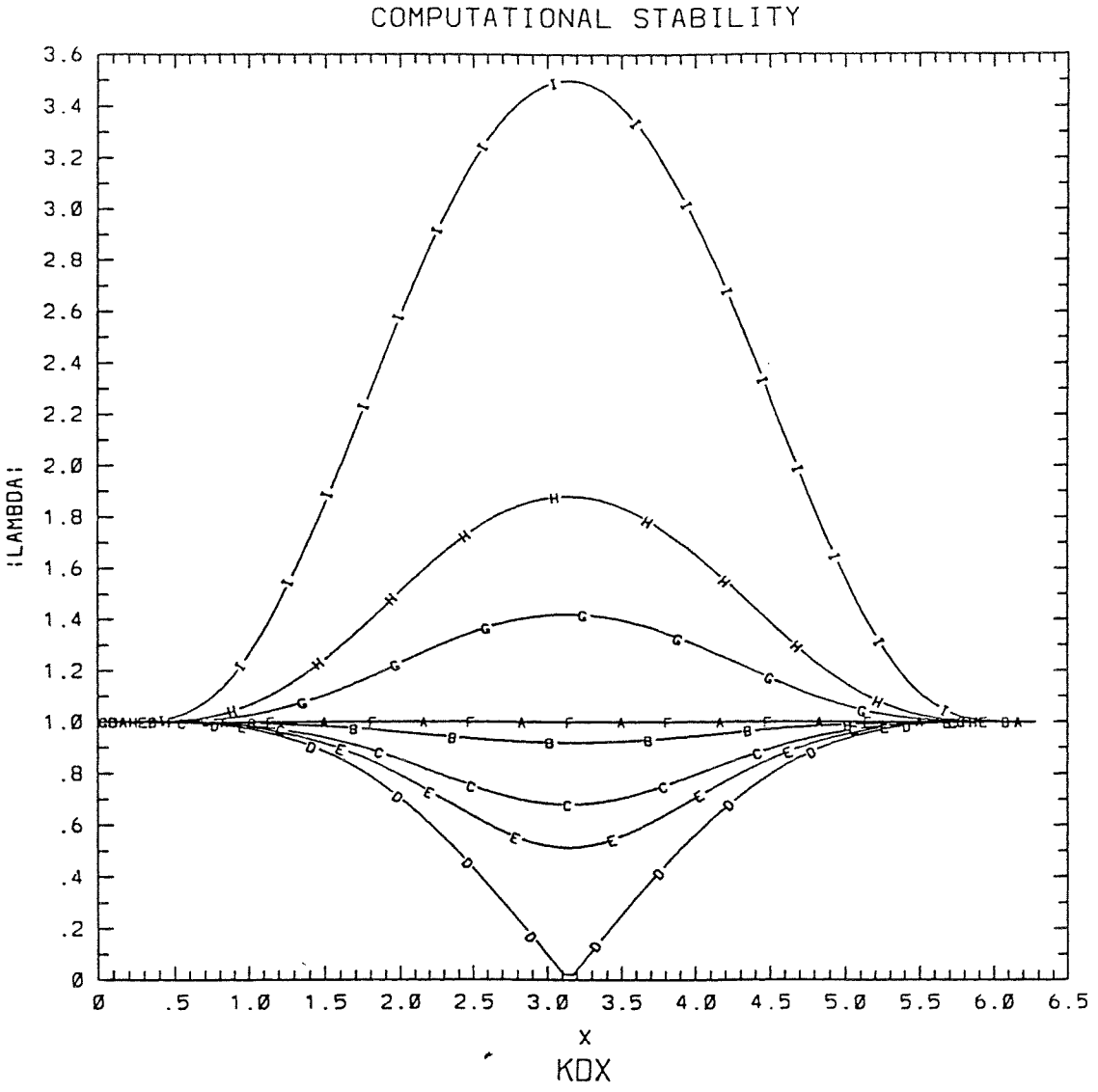

SECØND-ØRDER-EULER-UPSTREAM

1 b

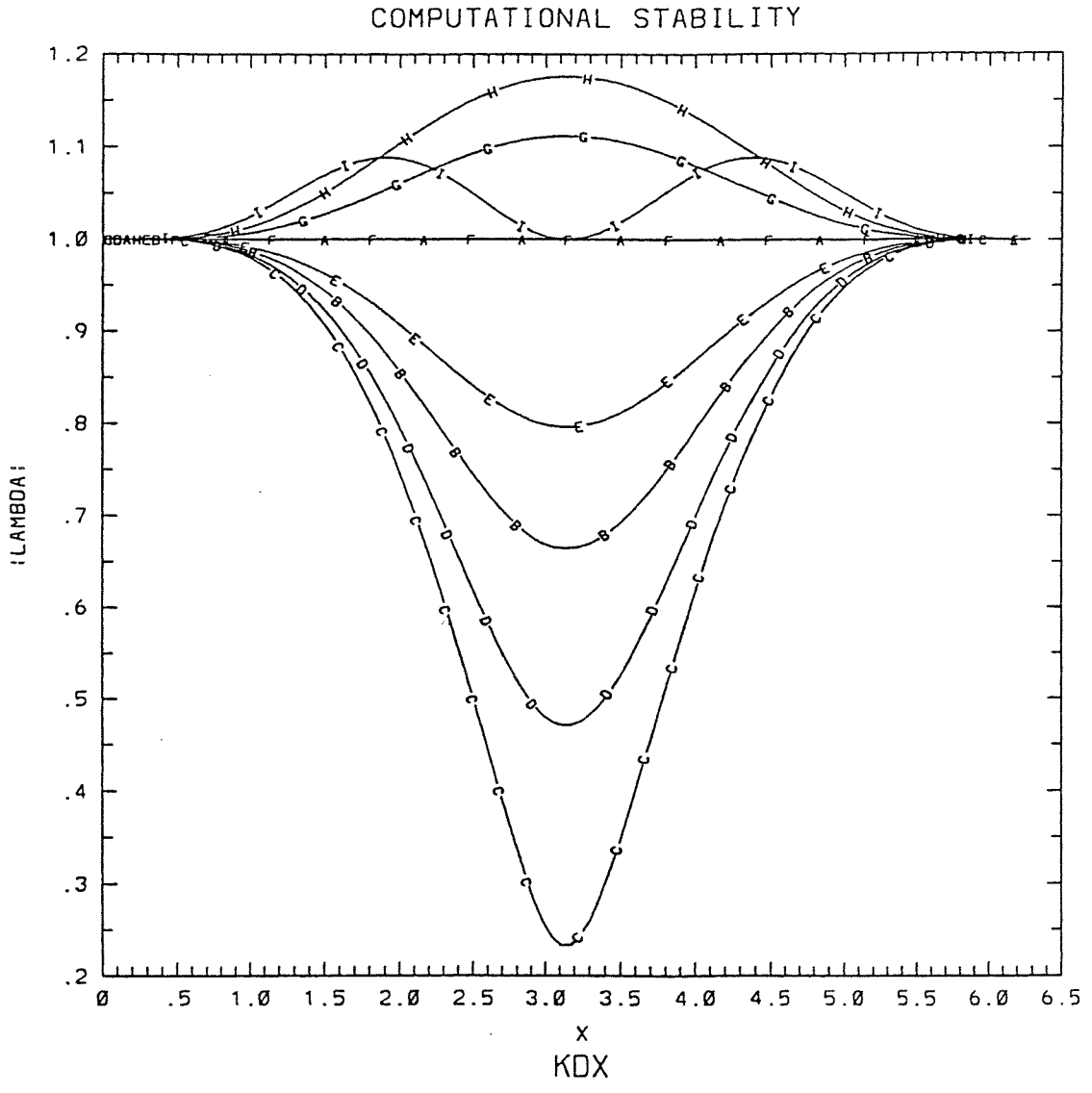
COMPUTATIONAL STABILITY
1.2
1.1
1.0
.9
.8
.7
.6
.5
.4
.3
.2
!LAMBDA!
0
.5
1.0
1.5
2.0
2.5
3.0
3.5
4.0
4.5
5.0
5.5
6.0
6.5
X
KDX
THIRD-ØRDER-EULER-UPSTREAM

1c

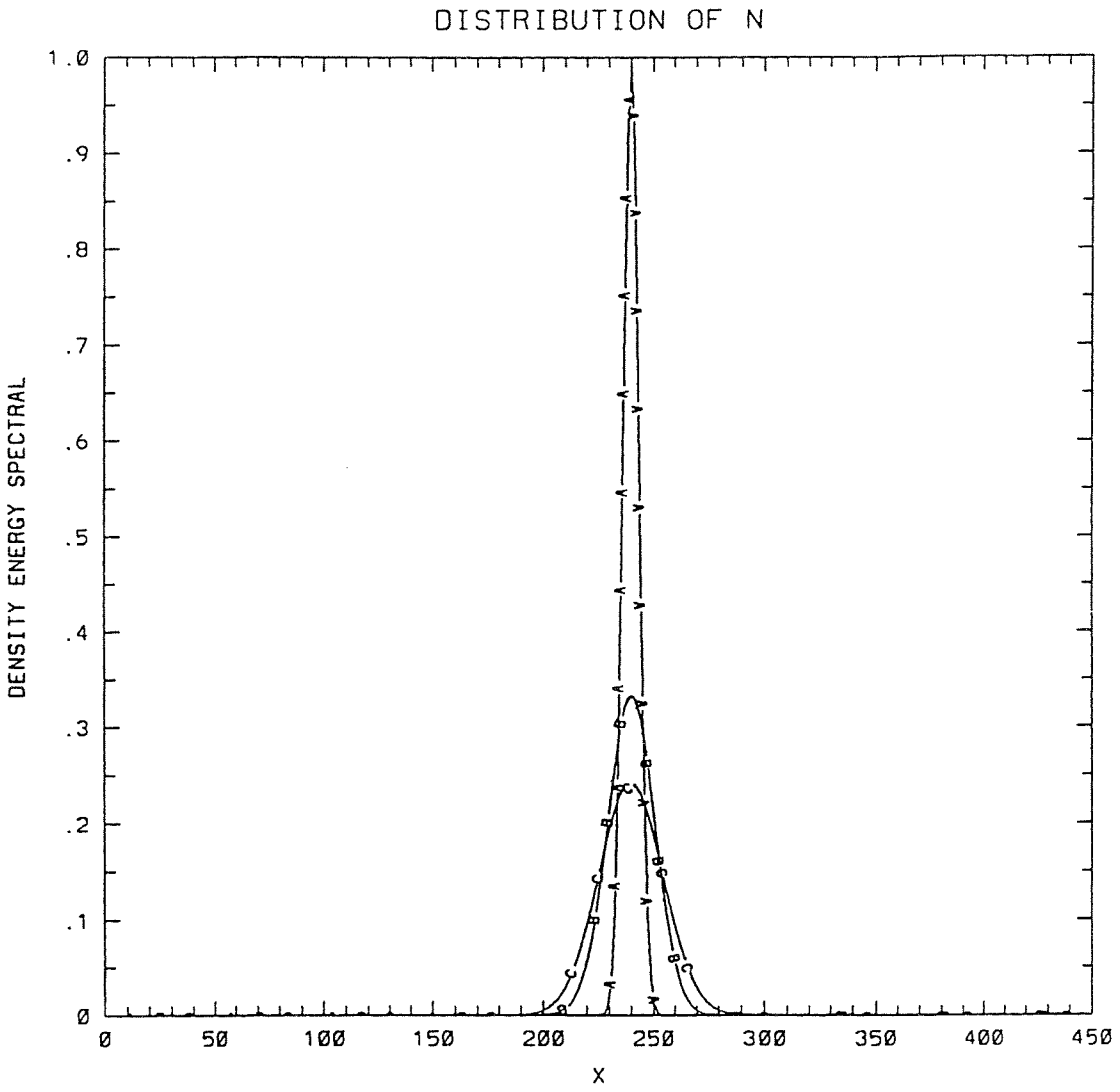

EULER-UPSTREAM

2a

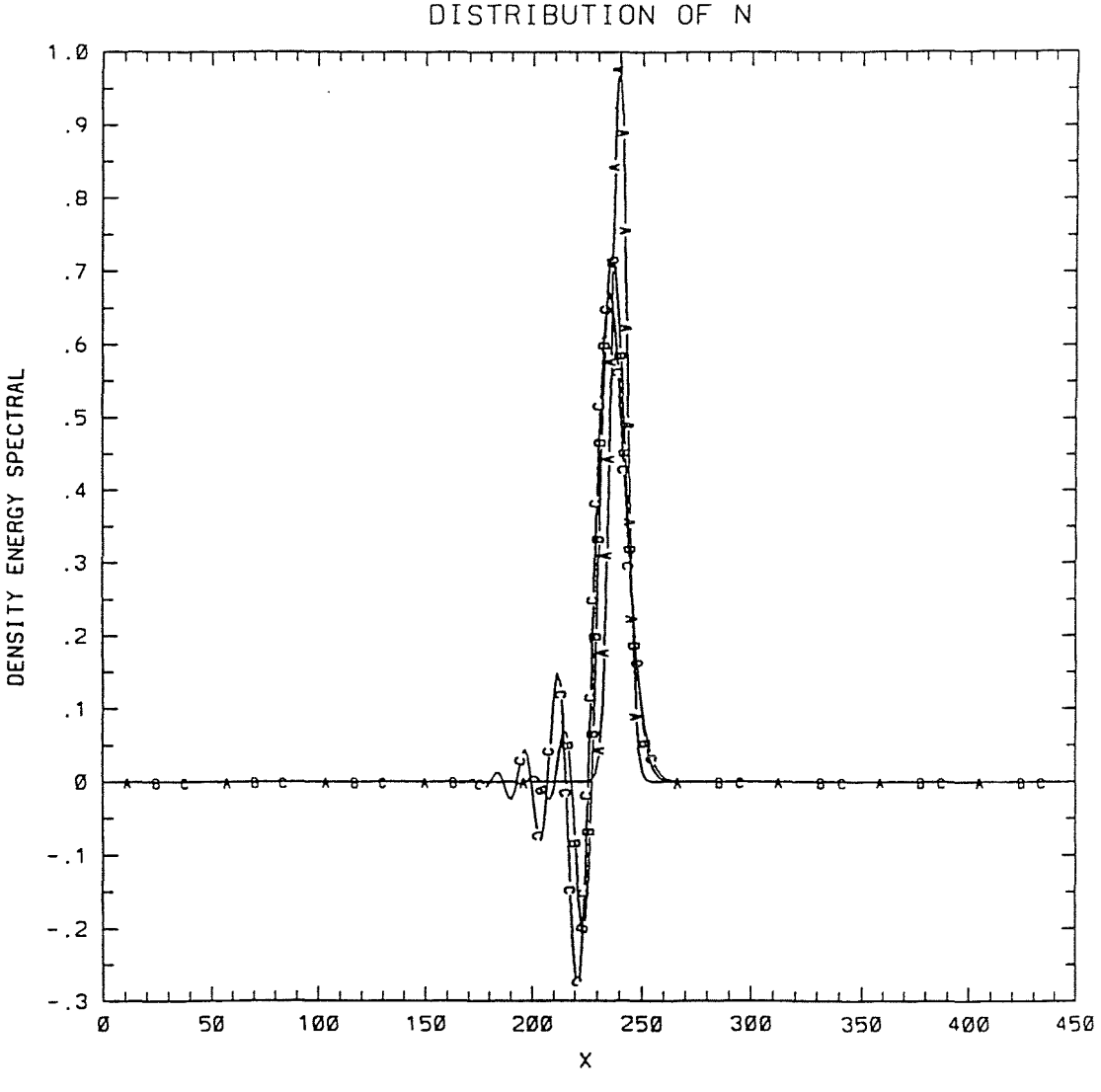

SECØND-ØRDER-UPSTREAM SCHEME

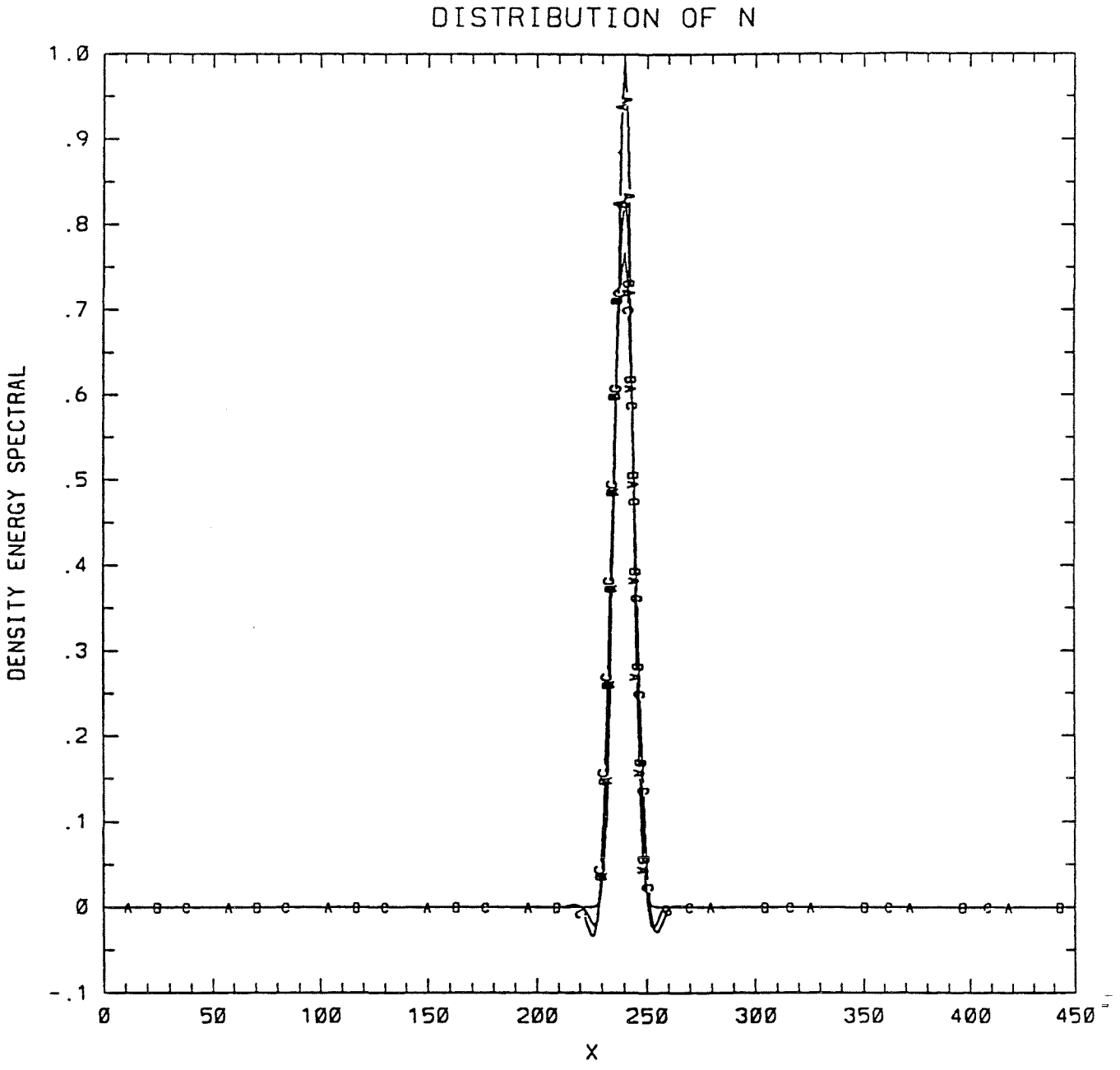

THIRD-ØRDER-UPSTREAM SCHEME

2c

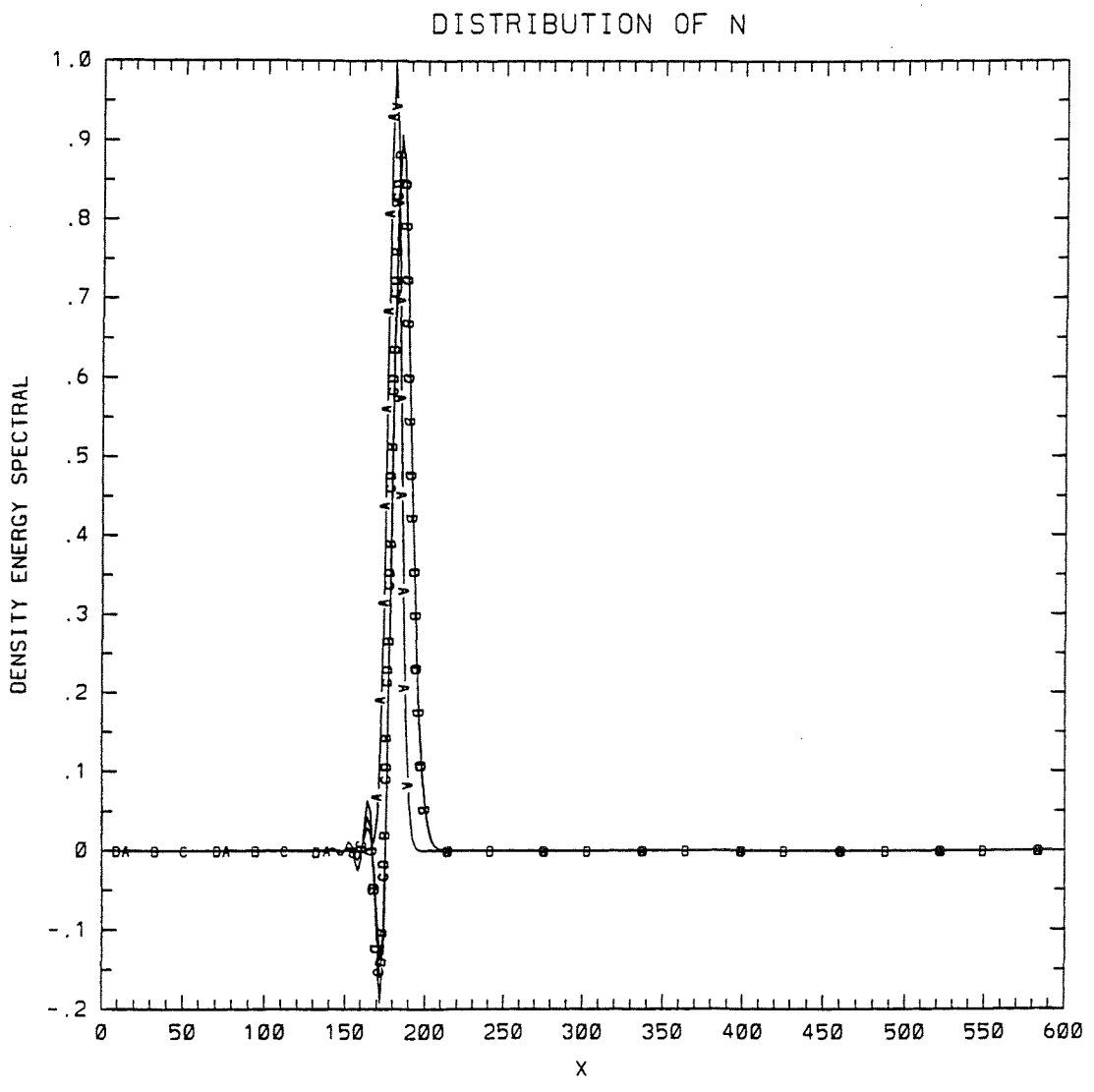

SECØND-ØRDER-UPSTREAM SCHEME

3a

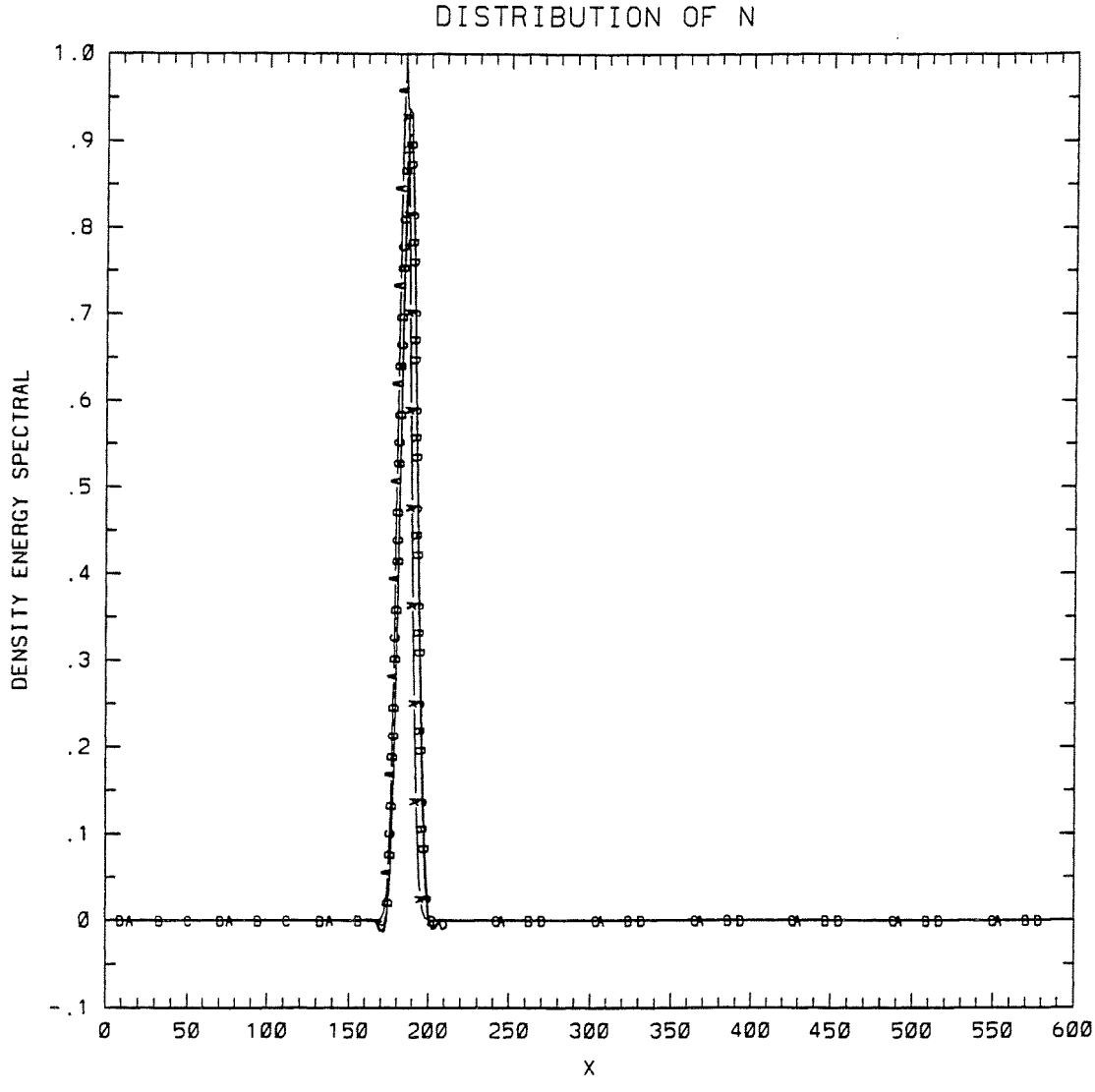

THIRD-ØRDER-UPSTREAM SCHEME

3b

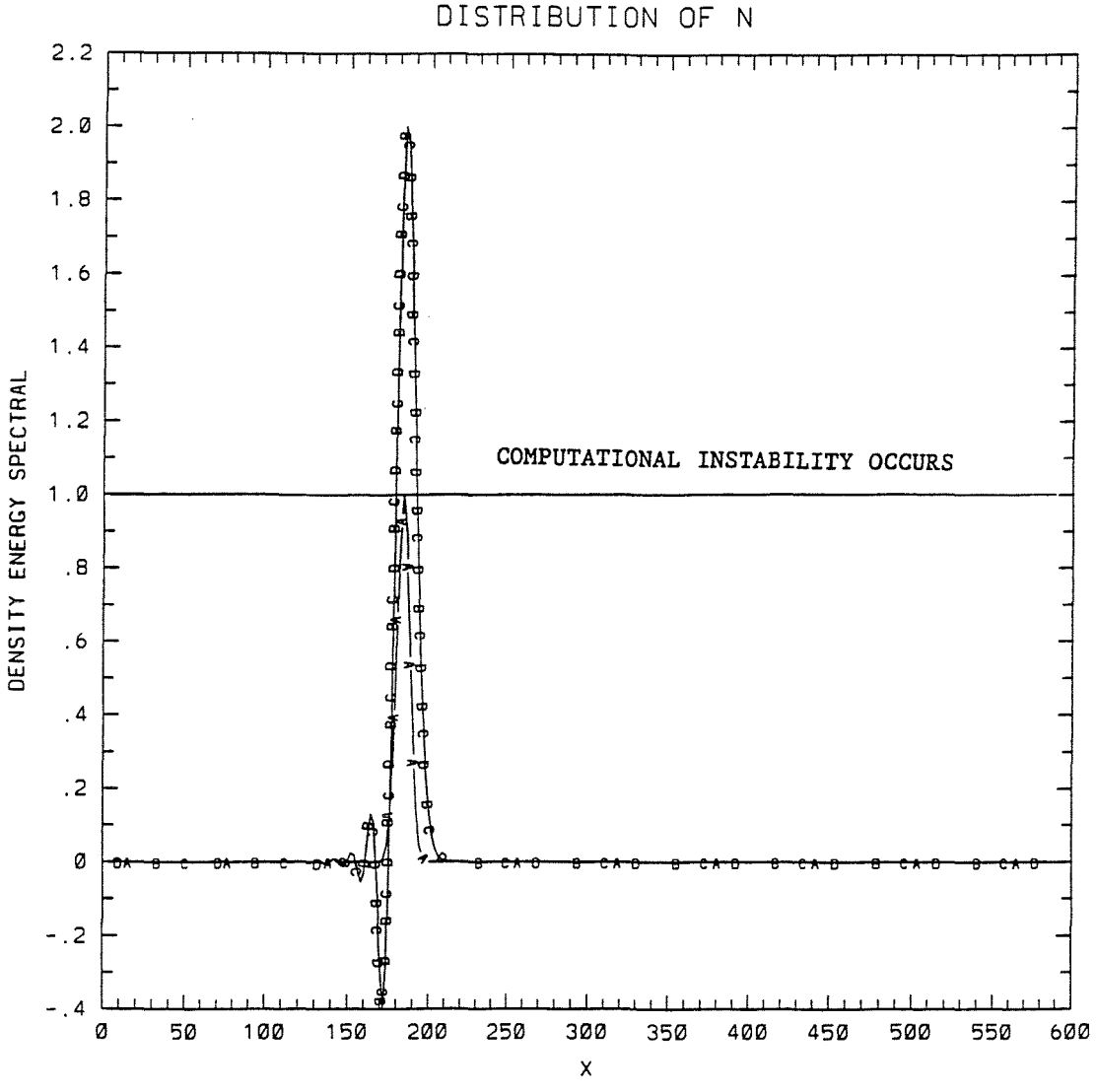

ICN SCHEME (ALPHA = 0)

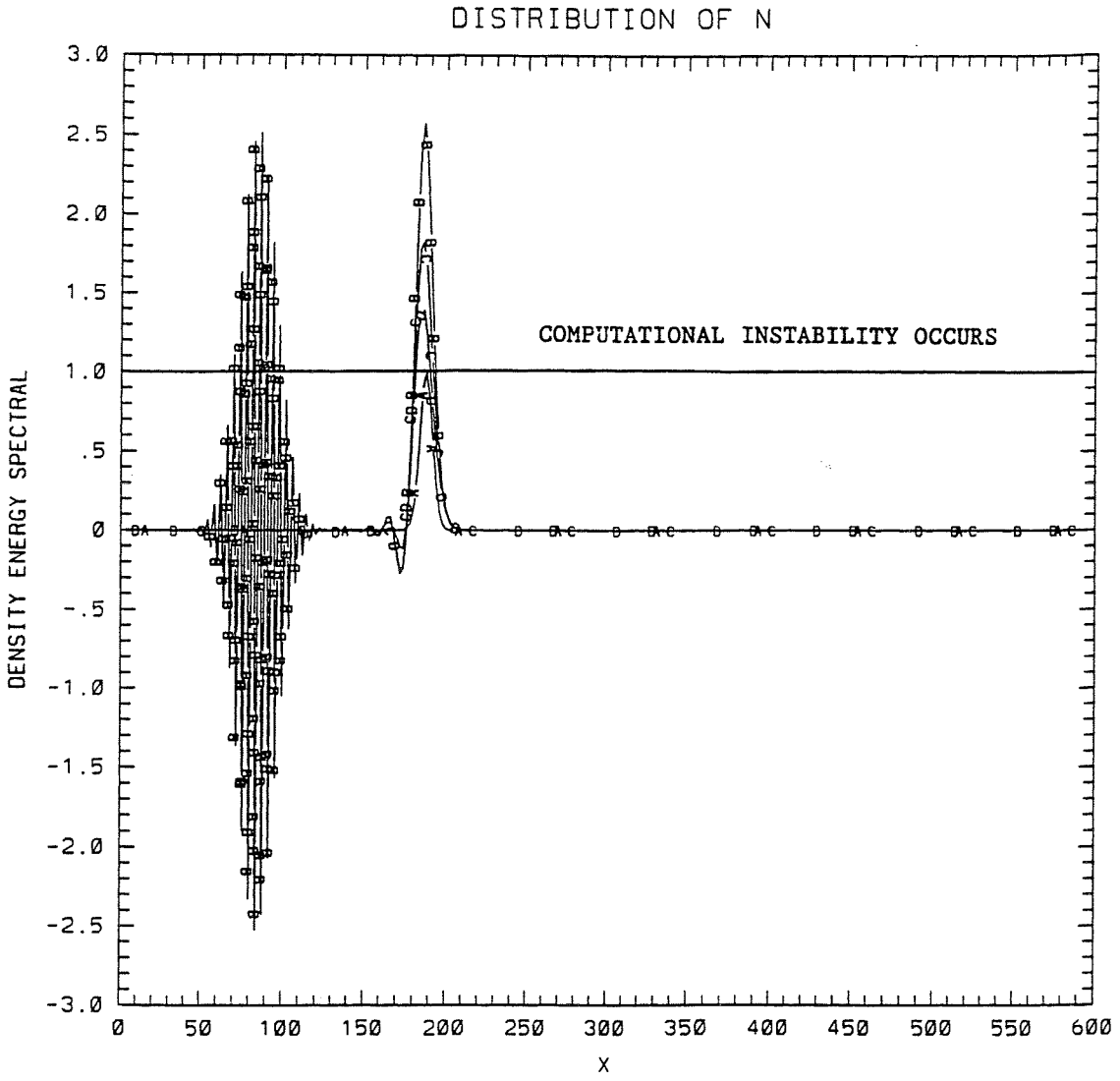

SECØND-ØRDER-UPSTREAM SCHEME

4a

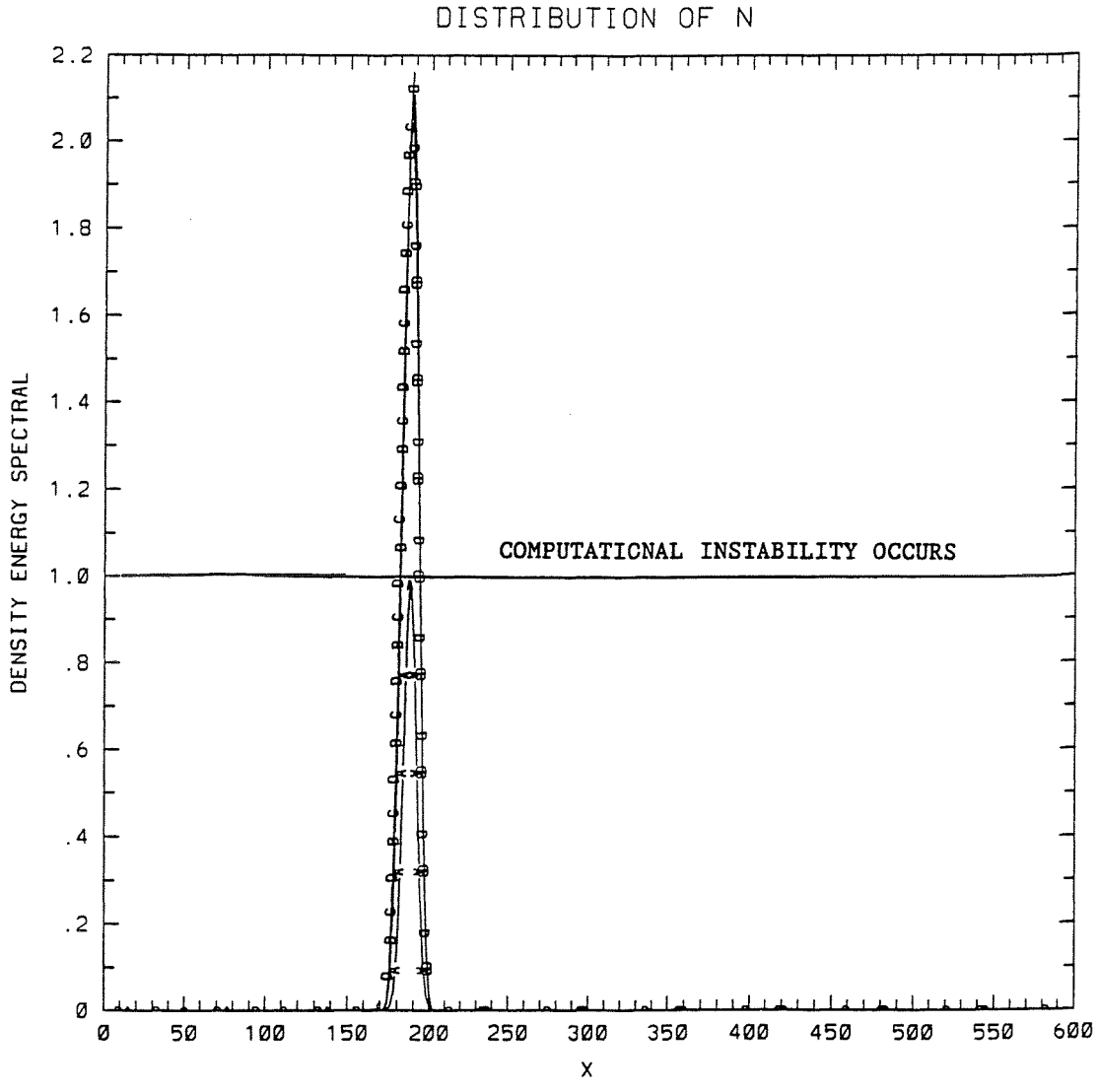

THIRD-ØRDER-UPSTREAM SCHEME

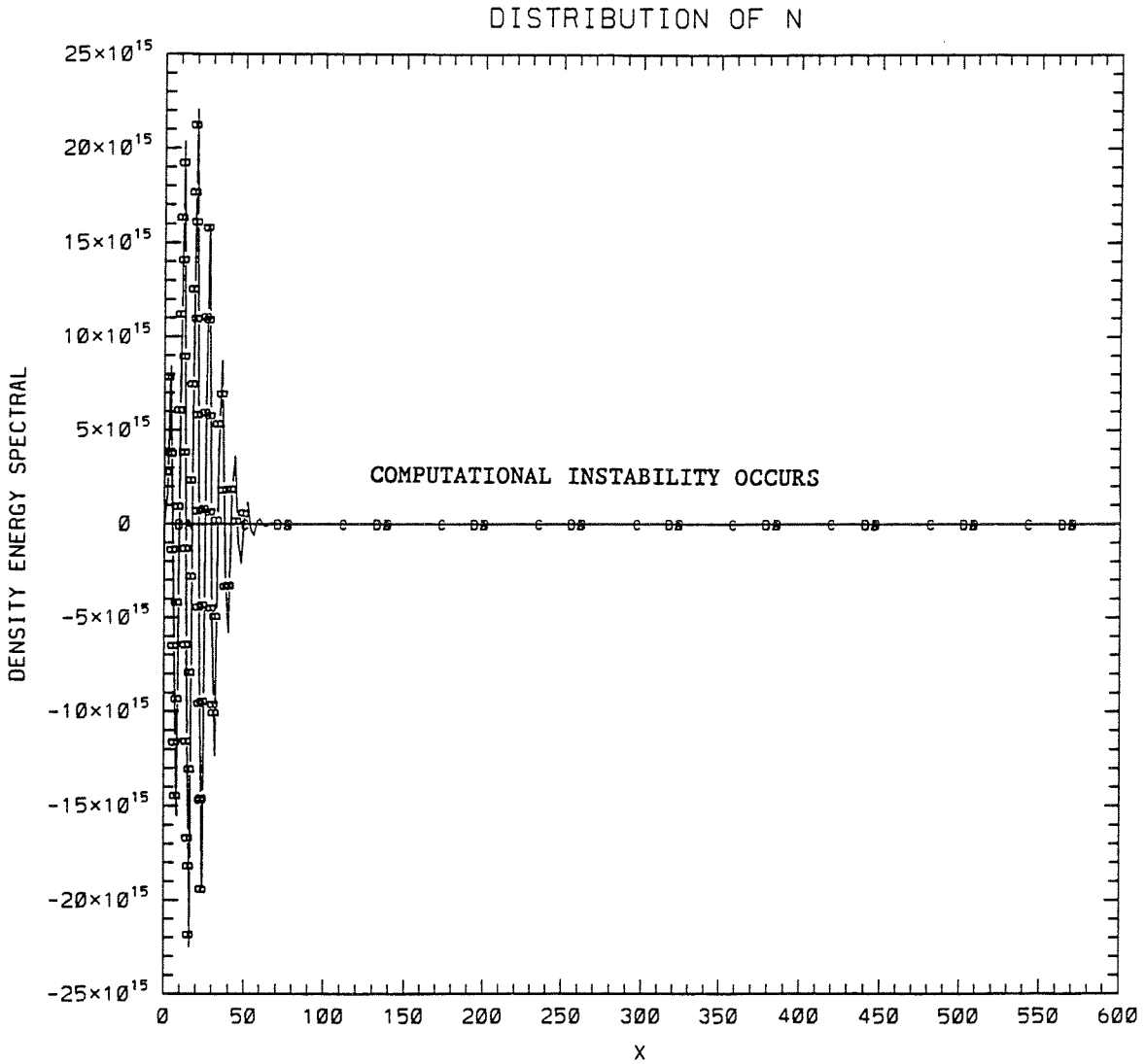

ICN SCHEME (ALPHA = 0)

4c

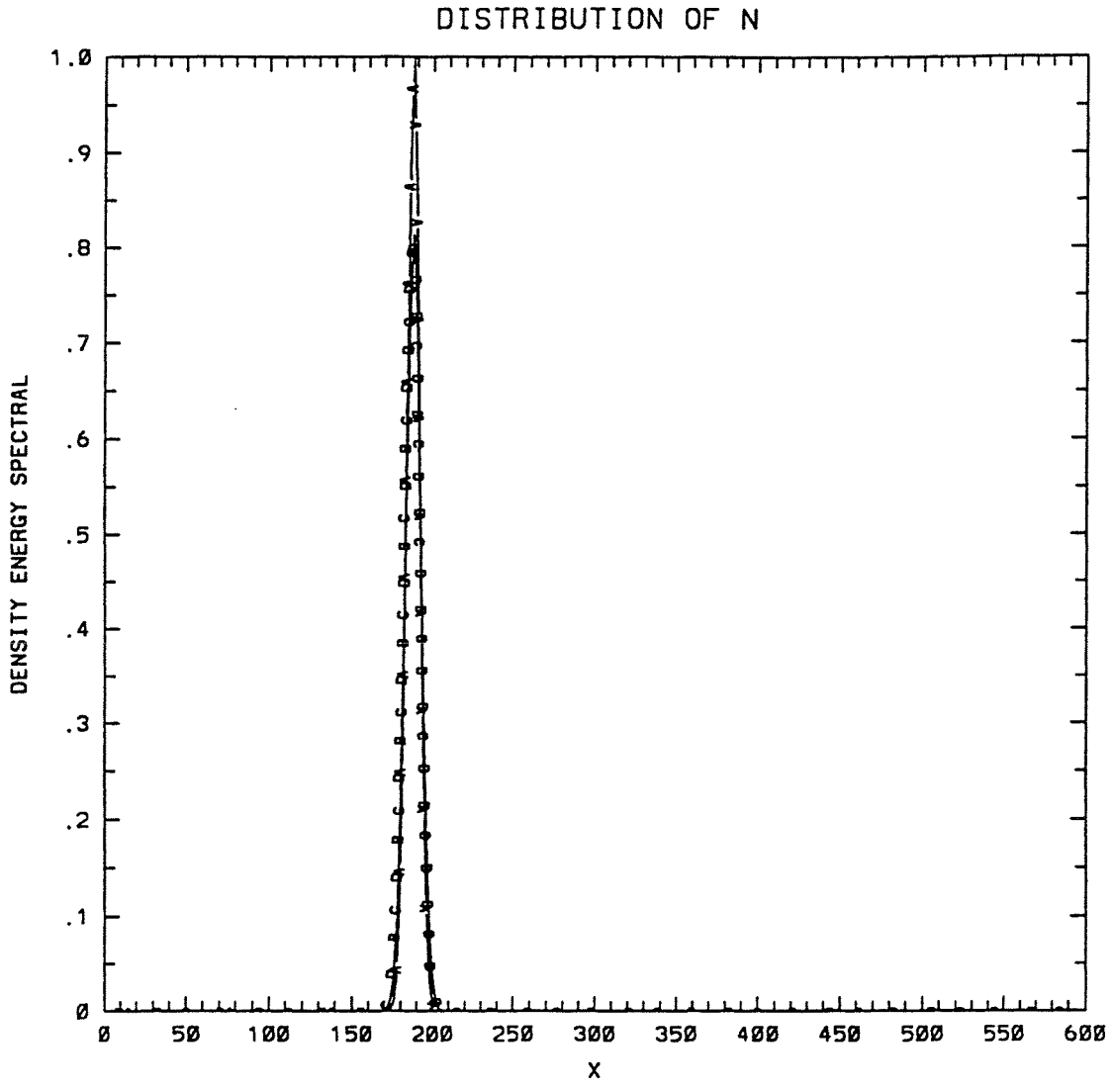
DISTRIBUTION OF N
DENSITY ENERGY SPECTRAL
1.0
.9
.8
.7
.6
.5
.4
.3
.2
.1
0
0
50
100
150
200
250
300
350
400
450
500
550
600
X

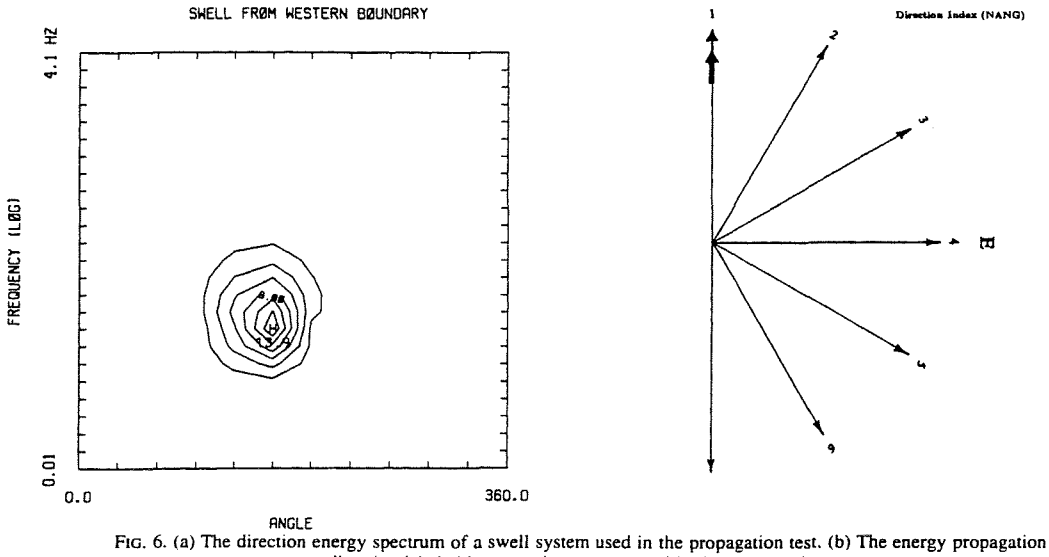

FIG. 6. (a) The direction energy spectrum of a swell system used in the propagation test. (b) The energy propagation direction labeled by a number system used in the computation.

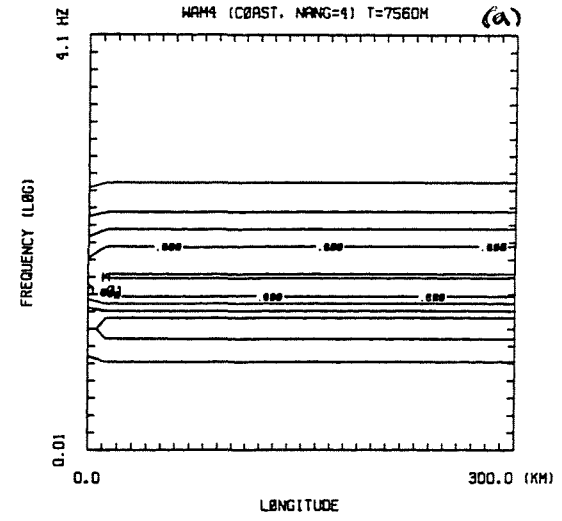
WAM4 (COAST, NANG=4) T=7560M
(a)
4.1 HZ
0.01
FREQUENCY (LOG)
0.0
300.0 (KM)
LONGITUDE

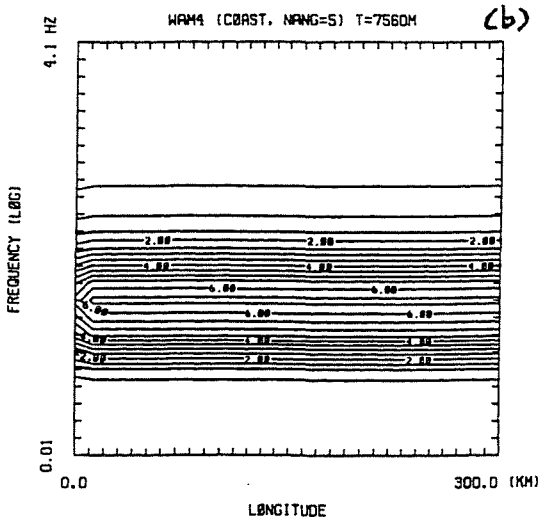
WAM4 (COAST, NANG=5) T=7560M
(b)
4.1 HZ
0.01
FREQUENCY (LOG)
0.0
300.0 (KM)
LONGITUDE

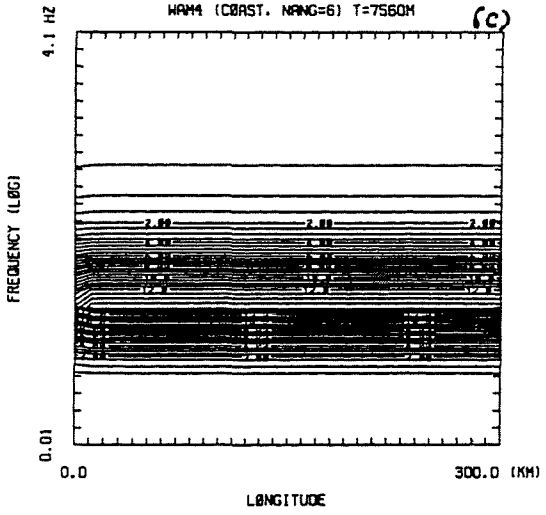
WAM4 (COAST, NANG=6) T=7560M
(c)
4.1 HZ
0.01
FREQUENCY (LOG)
0.0
300.0 (KM)
LONGITUDE

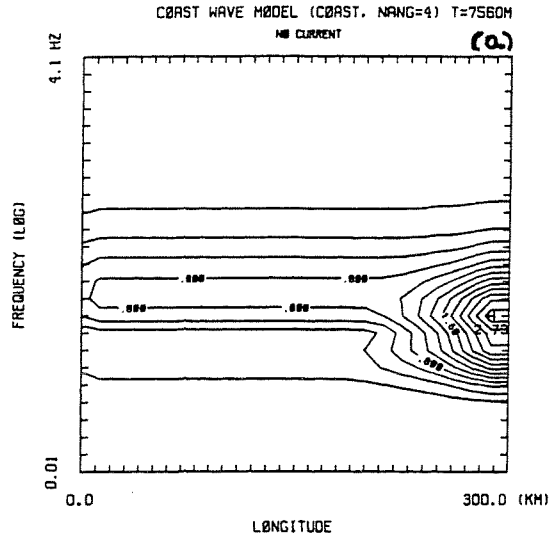
COAST WAVE MODEL (COAST, NANG=4) T=7560M
NB CURRENT
(a)
4.1 HZ
0.01
FREQUENCY (LOG)
0.0
300.0 (KM)
LONGITUDE

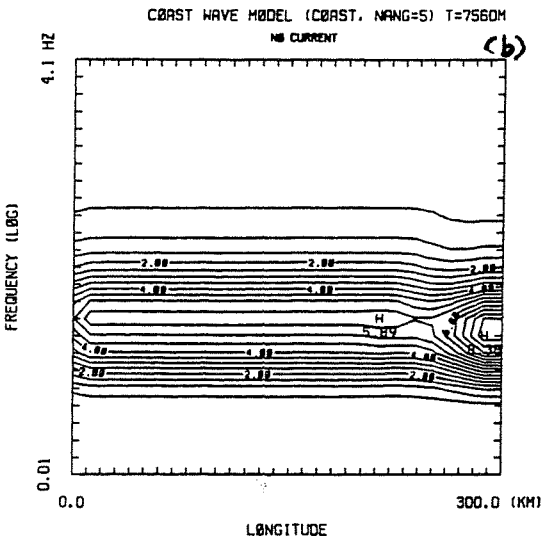
COAST WAVE MODEL (COAST, NANG=5) T=7560M
NB CURRENT
(b)
4.1 HZ
0.01
FREQUENCY (LOG)
0.0
300.0 (KM)
LONGITUDE

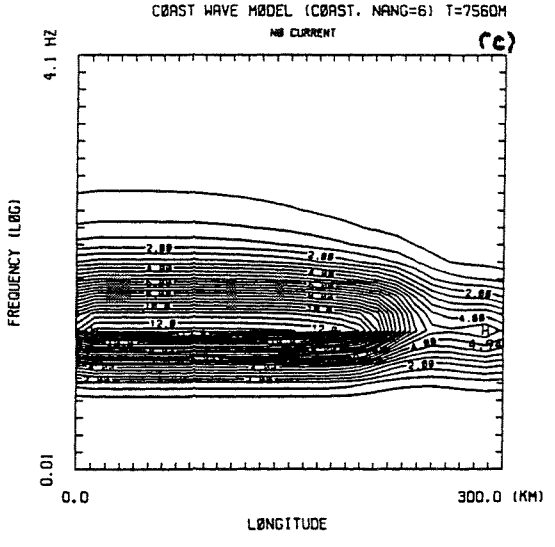
COAST WAVE MODEL (COAST, NANG=6) T=7560M
NB CURRENT
(c)
4.1 HZ
0.01
FREQUENCY (LOG)
0.0
300.0 (KM)
LONGITUDE

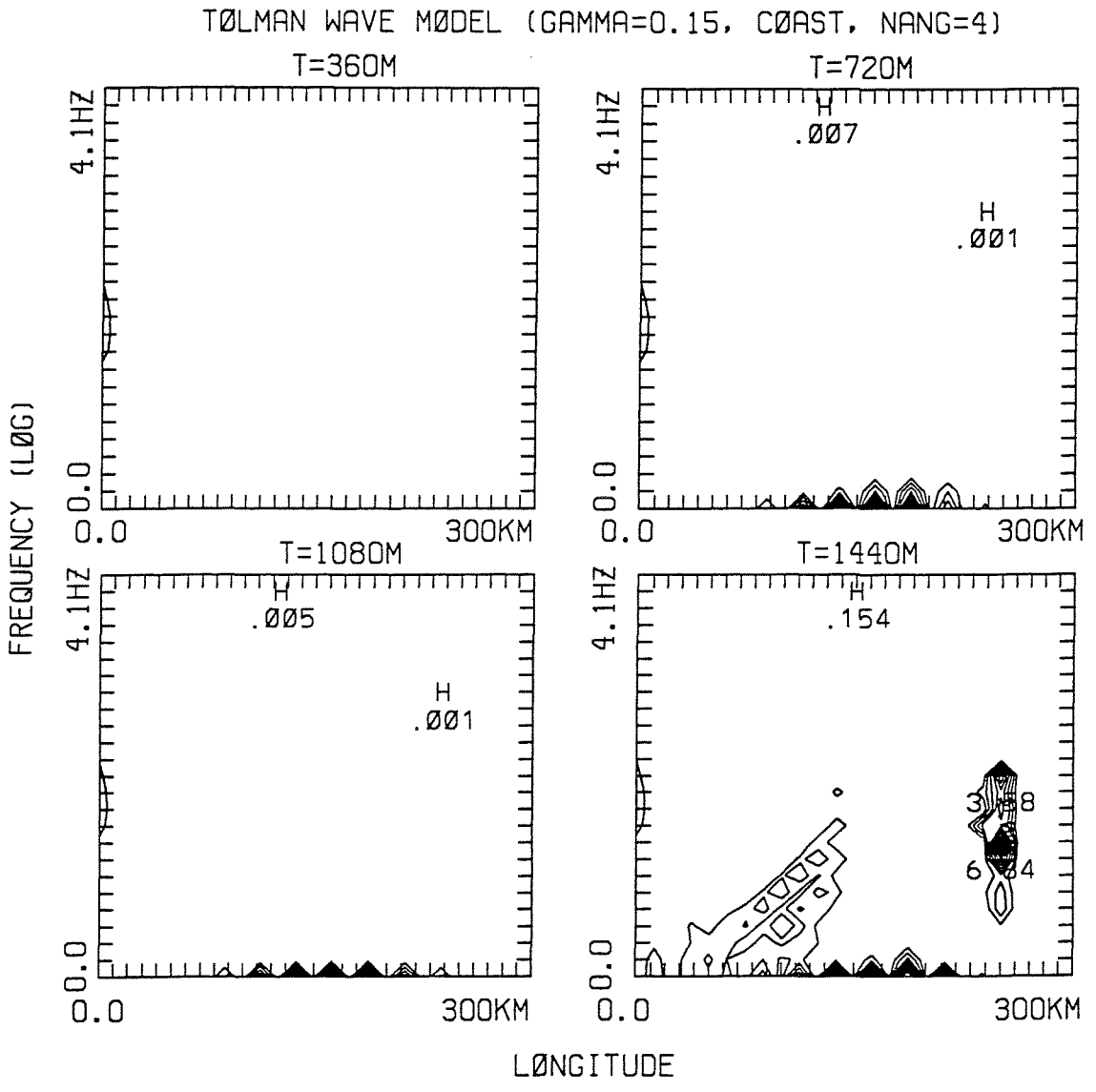
TØLMAN WAVE MØDEL (GAMMA=0.15, CØAST, NANG=4)
T=360M
T=720M
T=1080M
T=1440M
4.1HZ
0.0
300KM
H
.ØØ7
.ØØ1
.Ø05
.154
3
8
6
4
FREQUENCY (LØG)
LØNGITUDE

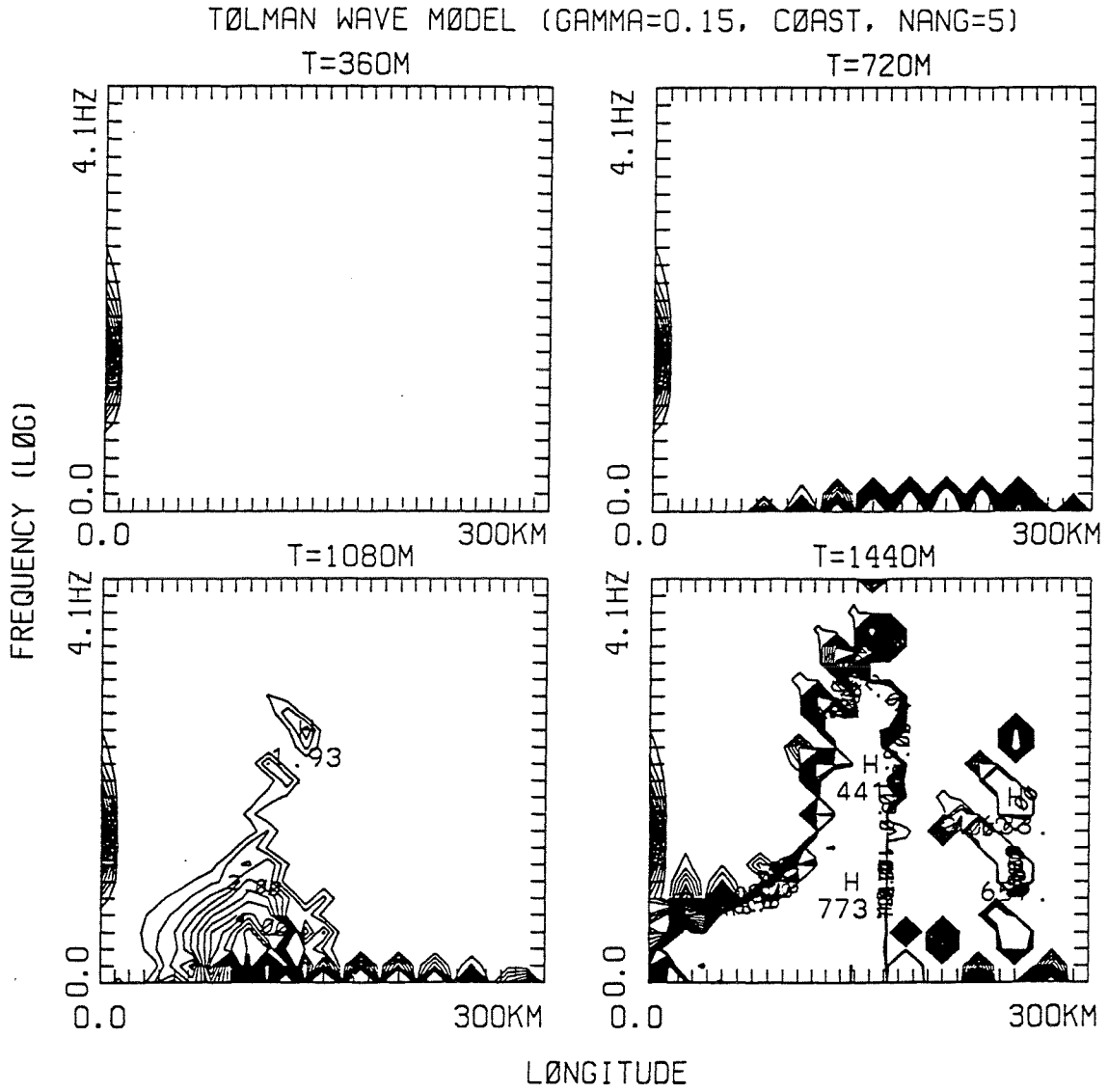
TØLMAN WAVE MØDEL (GAMMA=0.15, CØAST, NANG=5)
T=360M
T=720M
T=1080M
T=1440M
4.1HZ
0.0
300KM
FREQUENCY (LØG)
LØNGITUDE
H
44
H
773

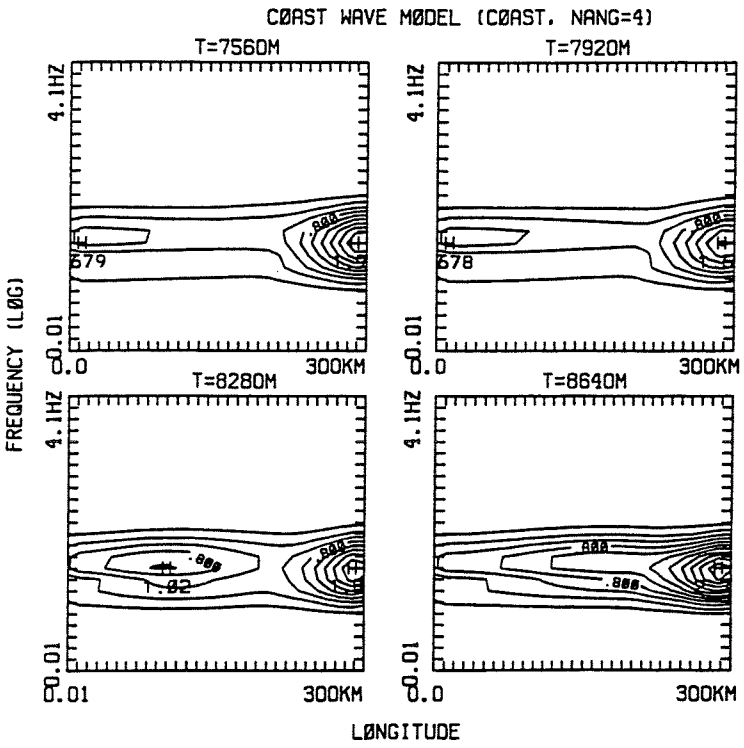
CØAST WAVE MØDEL (CØAST, NANG=4)
T=7560M
T=7920M
T=8280M
T=8640M
4.1HZ
0.01
0.0
300KM
FREQUENCY (LØG)
LØNGITUDE

10a

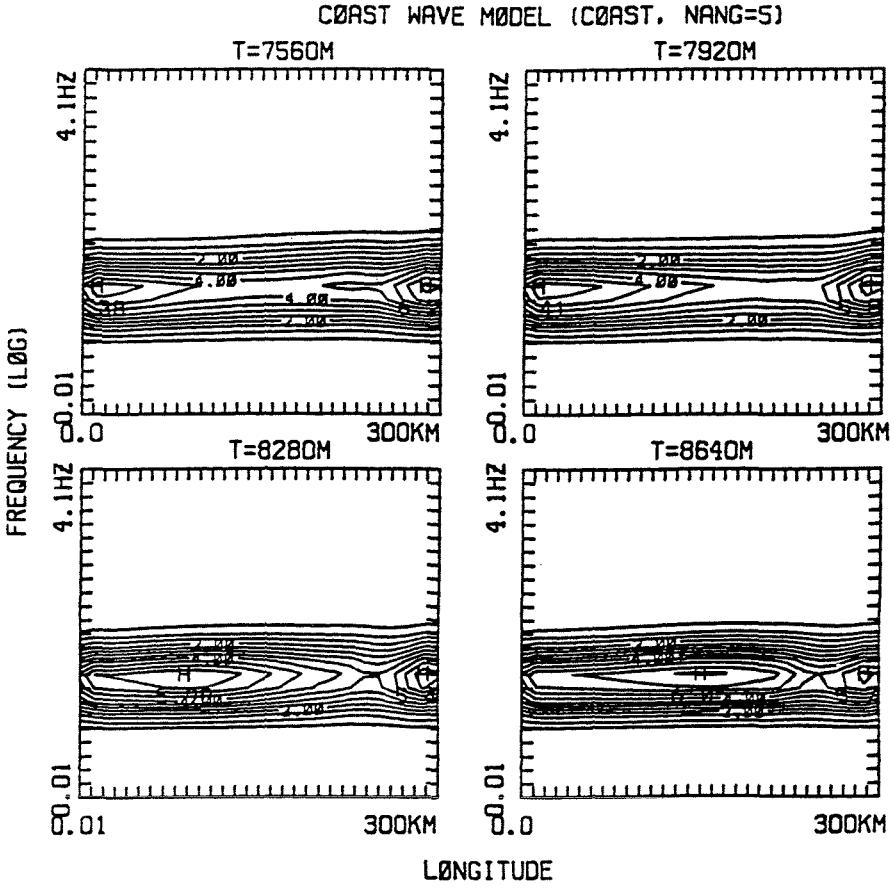
COAST WAVE MODEL (COAST, NANG=5)
T=7560M
T=7920M
T=8280M
T=8640M
4.1HZ
0.01
0.0
300KM
FREQUENCY (LOG)
LONGITUDE

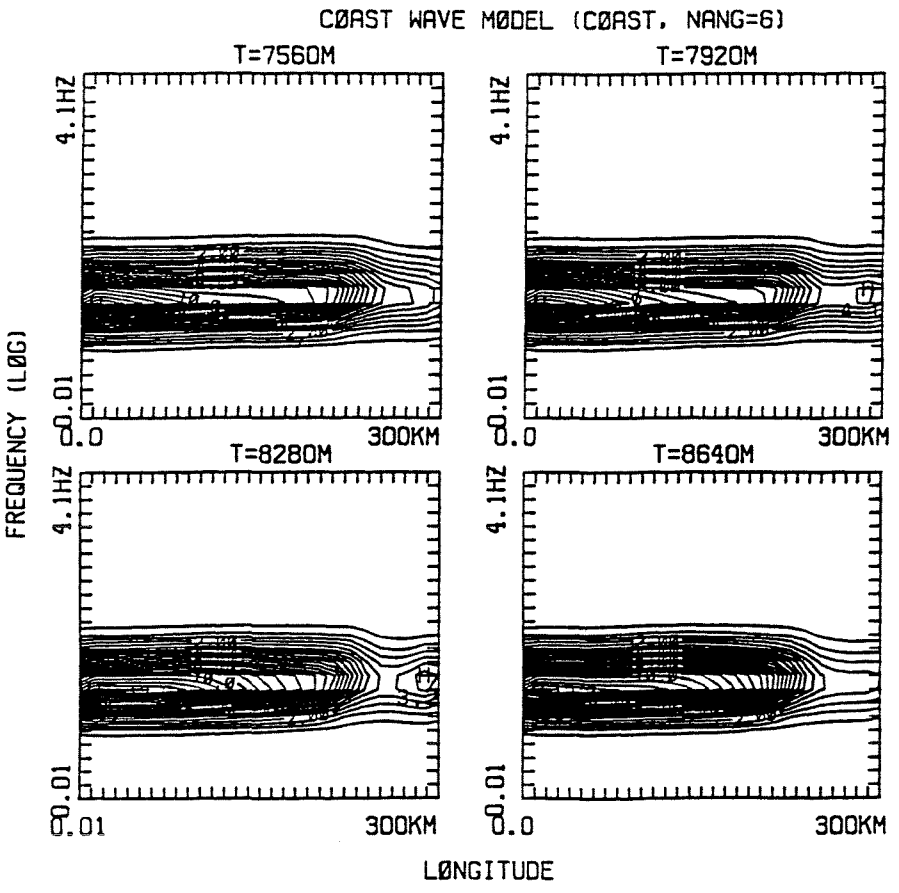
CØAST WAVE MØDEL (CØAST, NANG=6)
T=7560M
T=7920M
T=8280M
T=8640M
4.1HZ
0.01
0.0
300KM
FREQUENCY (LØG)
LØNGITUDE

10 c

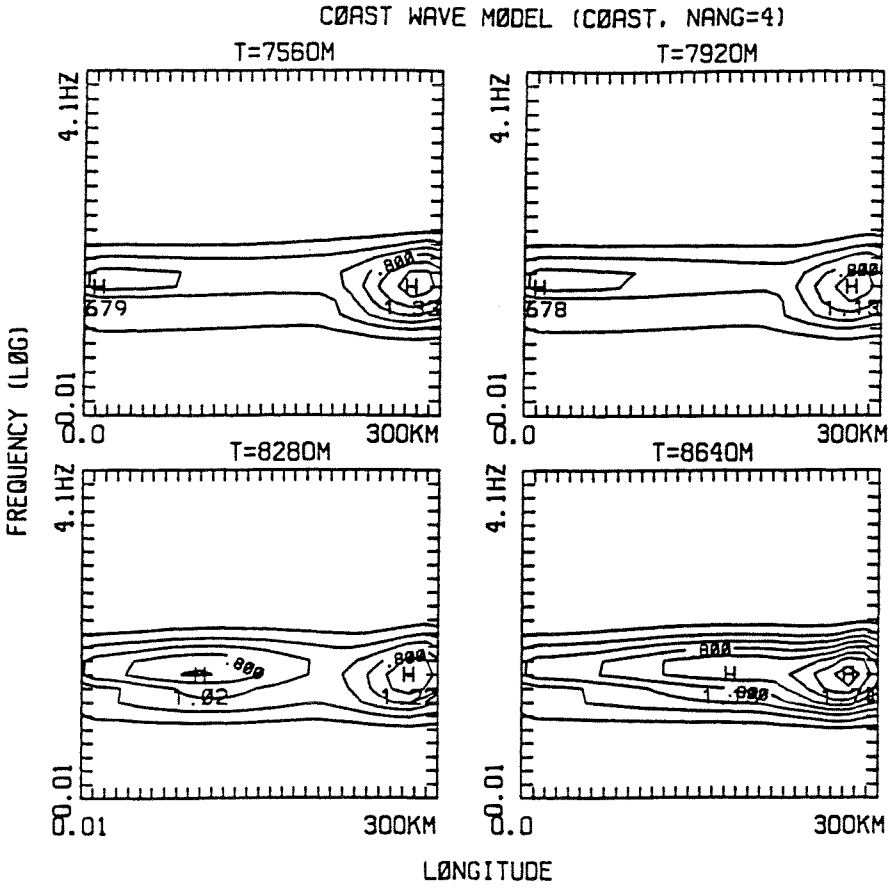
CØAST WAVE MØDEL (CØAST, NANG=4)
T=7560M
T=7920M
T=8280M
T=8640M
4.1HZ
0.01
0.0
300KM
.01
FREQUENCY (LØG)
LØNGITUDE
H
L
.800
.679
.678
1.02

11a

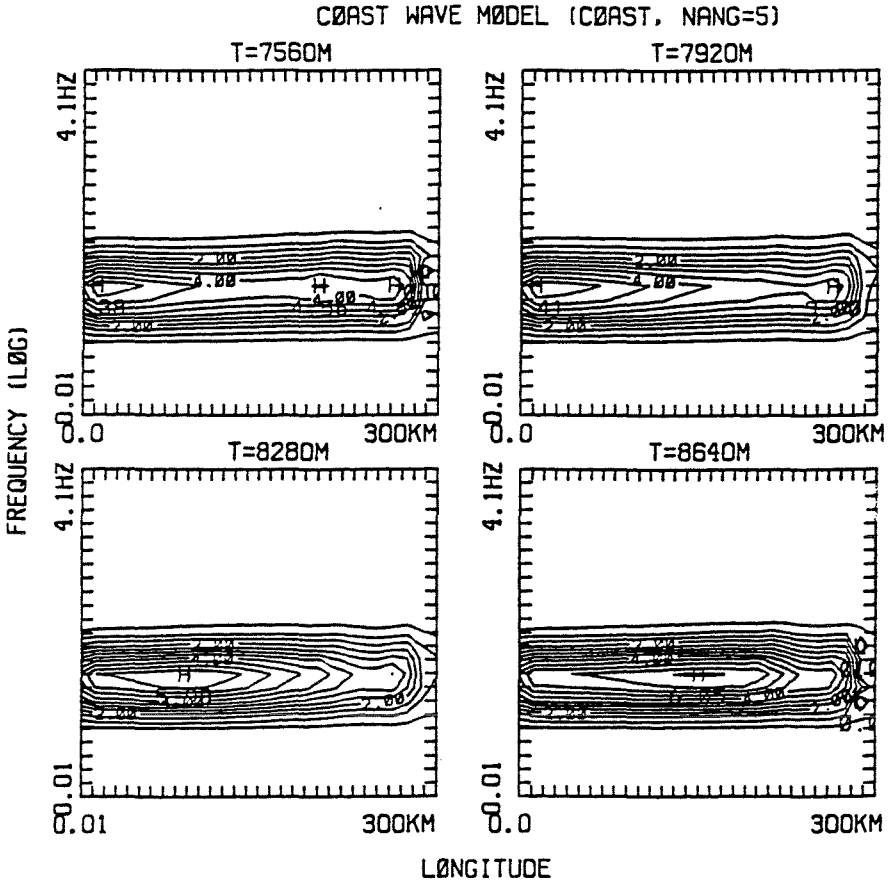
CØAST WAVE MØDEL (CØAST, NANG=5)
T=7560M
T=7920M
T=8280M
T=8640M
4.1HZ
0.01
0.0
300KM
0.01
FREQUENCY (LØG)
LØNGITUDE

11 b

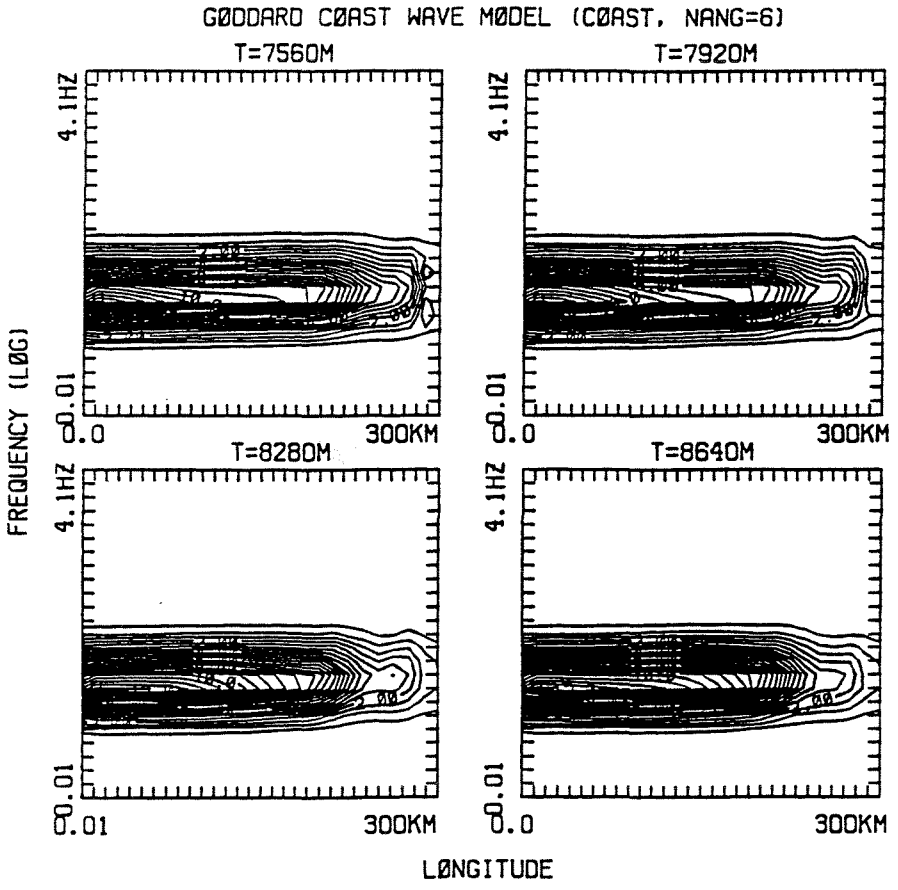
GØDDARD CØAST WAVE MØDEL (CØAST, NANG=6)
T=7560M
T=7920M
T=8280M
T=8640M
4.1HZ
0.01
0.0
300KM
0.01
FREQUENCY (LØG)
LØNGITUDE

11 C

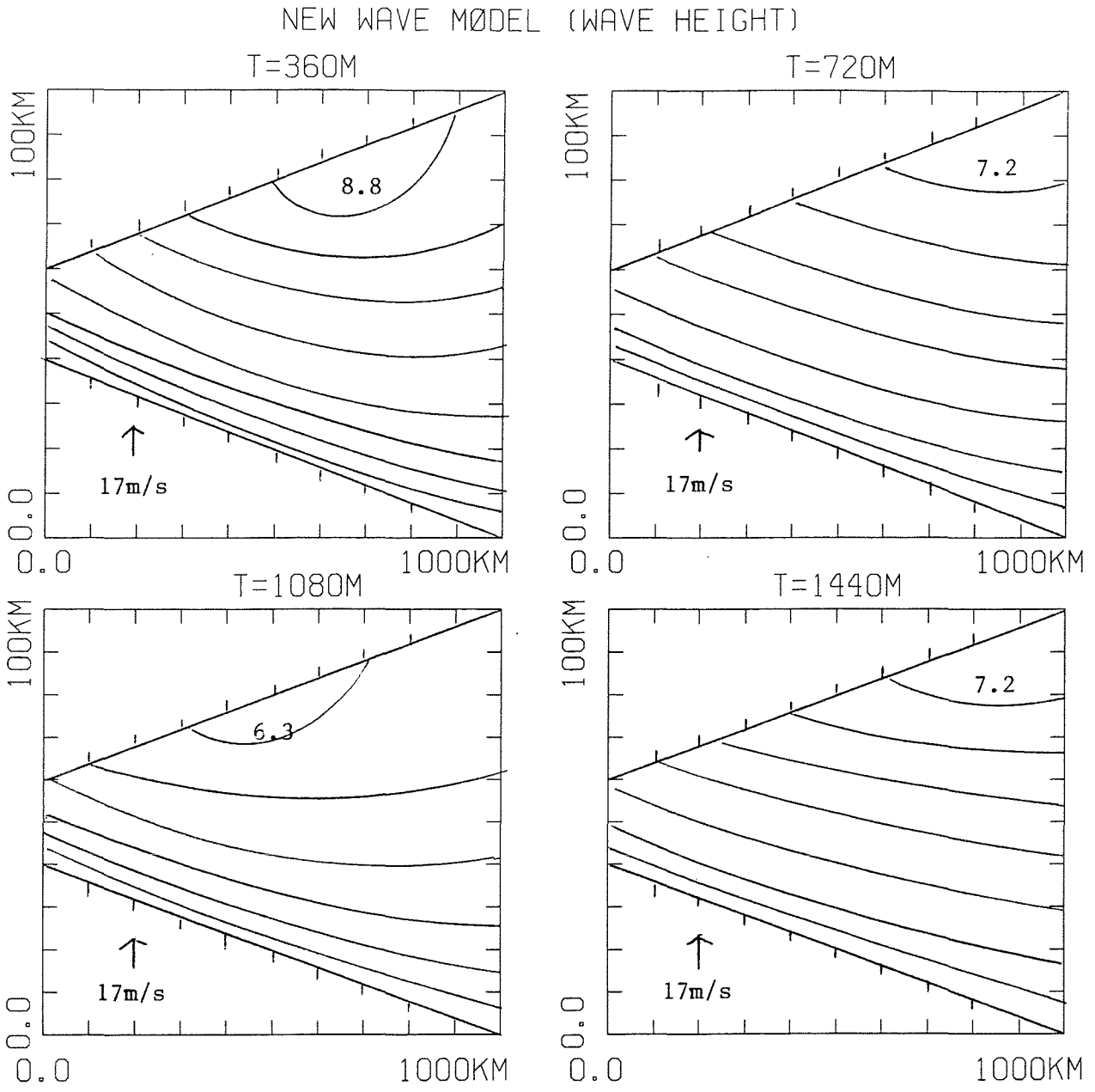

CONTOUR FROM 0100000E+00 TO -200000 CONTOUR INTERVAL OF 200000 PT(3,3)= 2.8829

12 a

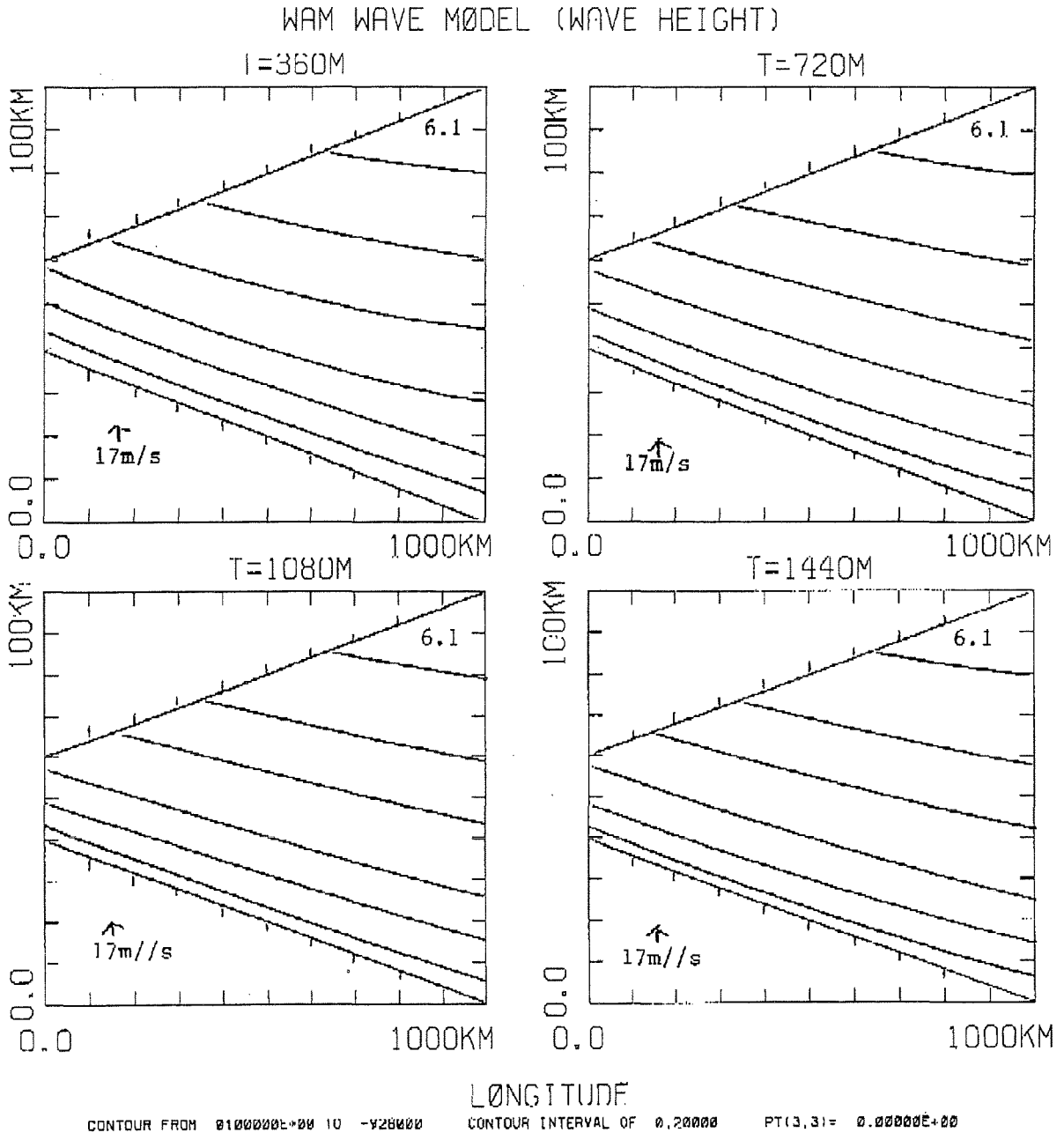
WAM WAVE MØDEL (WAVE HEIGHT)
T=360M
T=720M
T=1080M
T=1440M
100KM
0.0
1000KM
6.1
17m/s
17m//s
LØNGITUDE
CONTOUR FROM 0100000E+00 TO -926000
CONTOUR INTERVAL OF 0.20000
PT(3,3)= 0.000000E+00

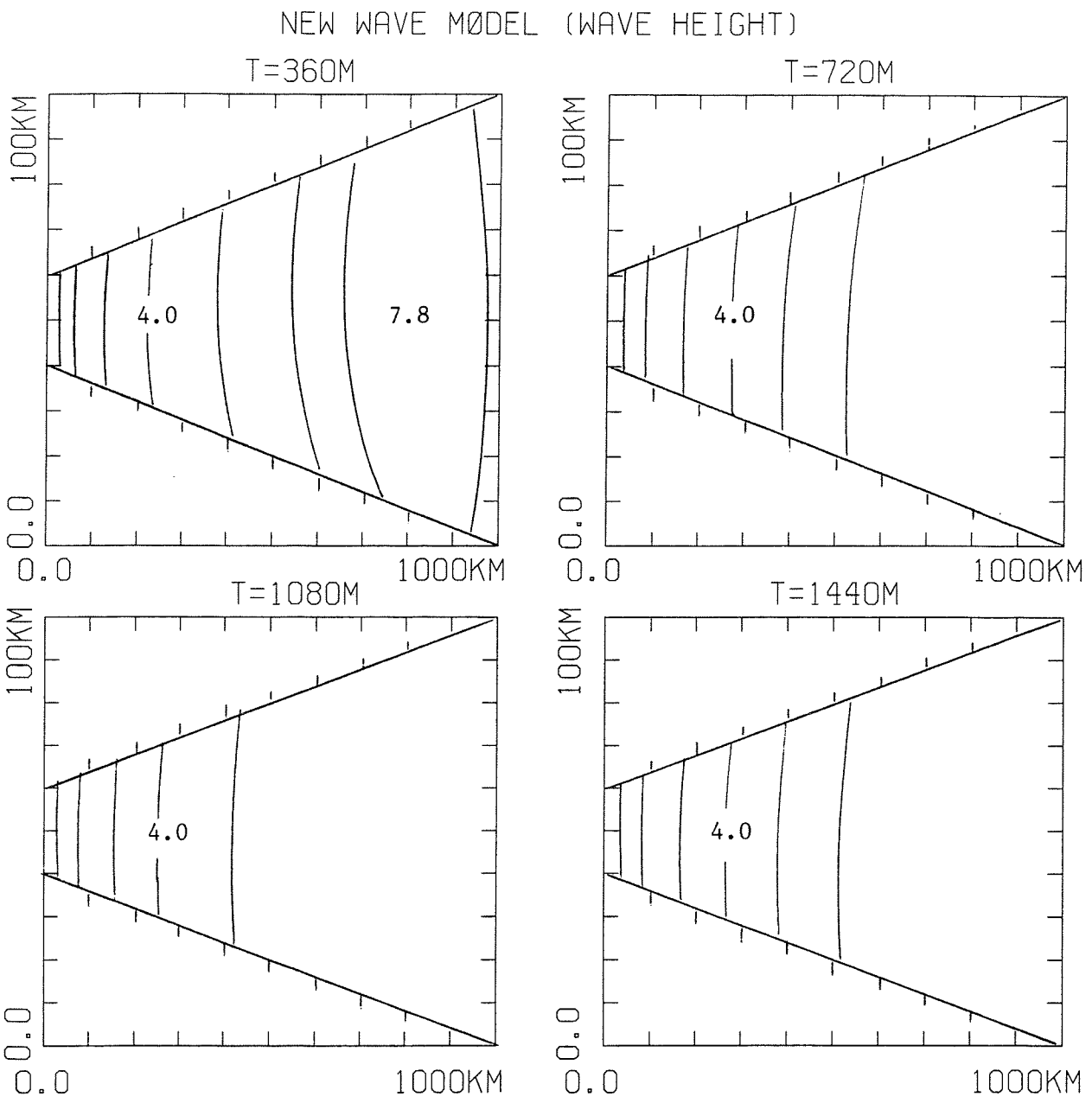
NEW WAVE MØDEL (WAVE HEIGHT)
T=360M
T=720M
T=1080M
T=1440M
100KM
0.0
1000KM
4.0
7.8
CONTOUR FROM 0100000E+00 TO -200000 CONTOUR INTERVAL OF 200000 PT(3,3)= 2.0000
17m/s

13a

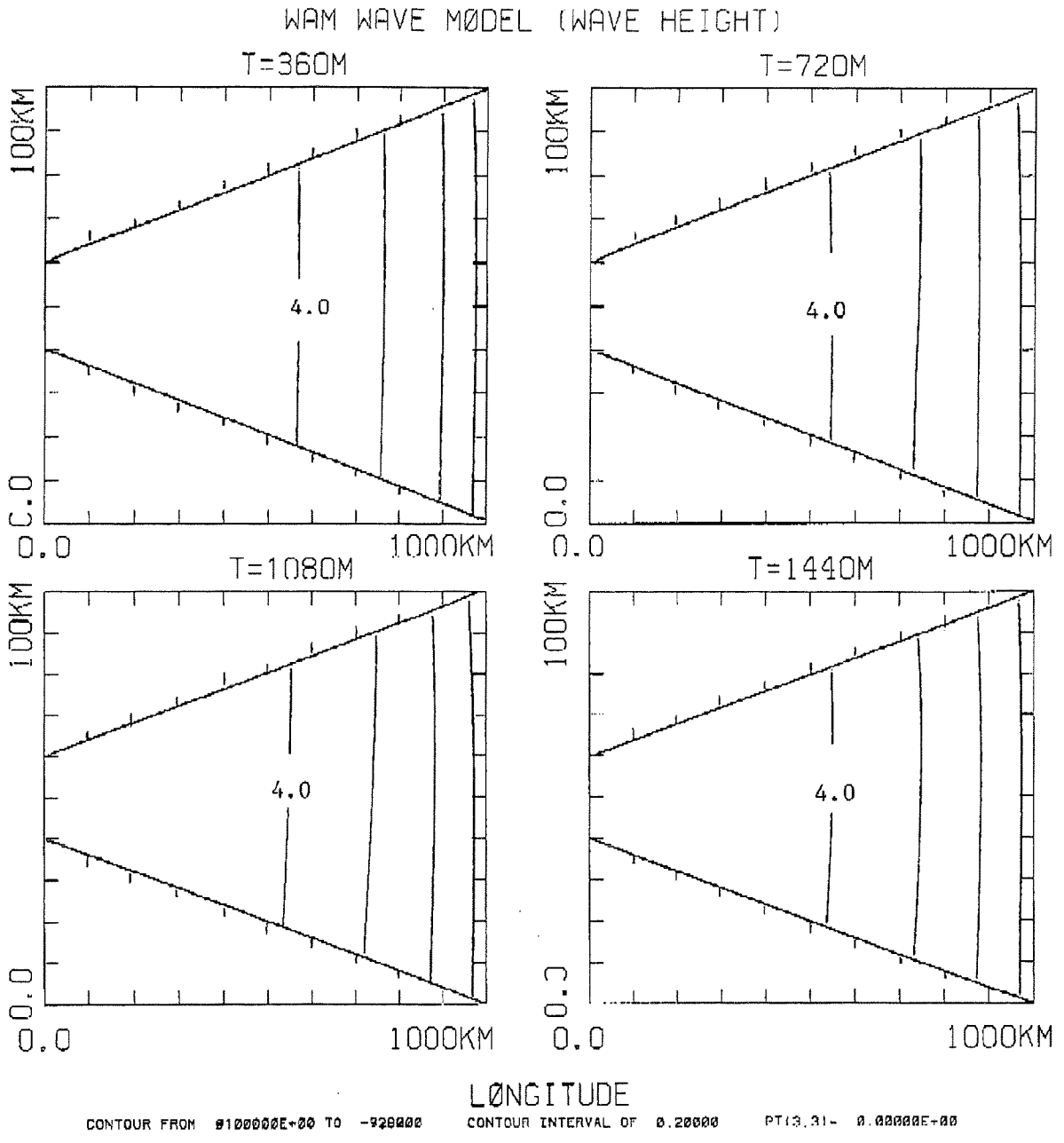
WAM WAVE MØDEL (WAVE HEIGHT)
T=360M
T=720M
T=1080M
T=1440M
100KM
0.0
1000KM
4.0
LØNGITUDE
CONTOUR FROM 0100000E+00 TO -920000
CONTOUR INTERVAL OF 0.20000
PT(3,3)= 0.00000E+00
17m/s

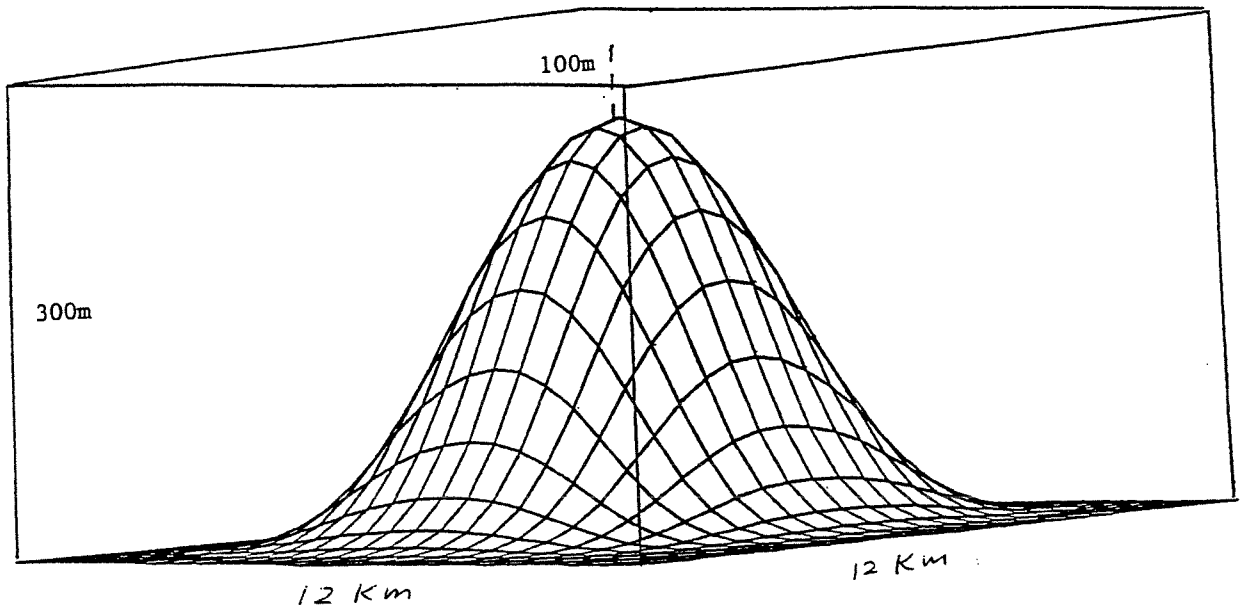

15 a

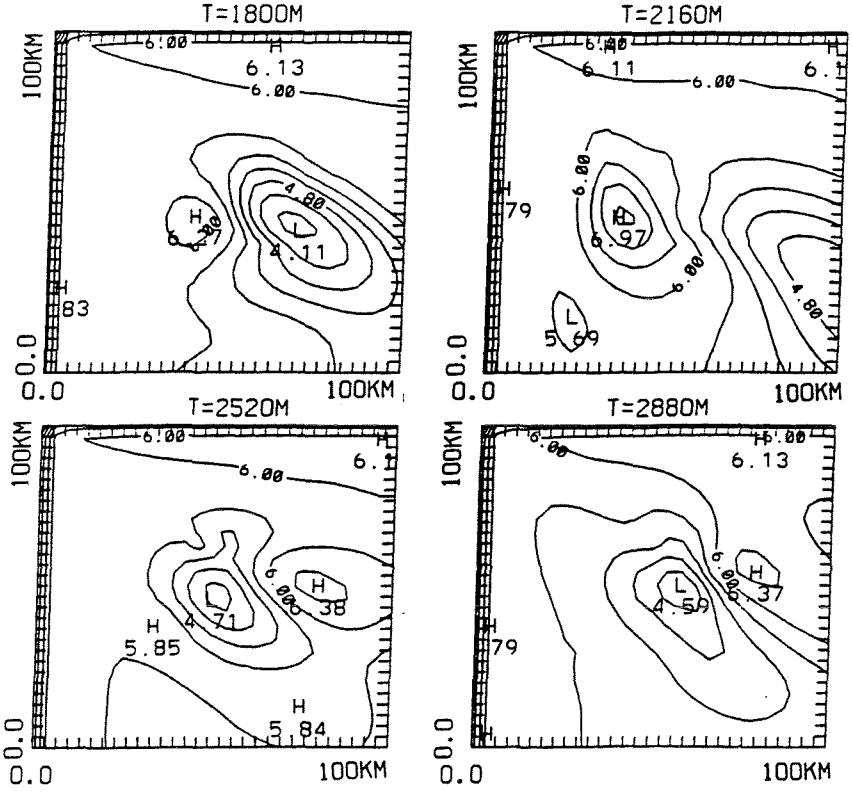
T=1800M
T=2160M
T=2520M
T=2880M
100KM
0.0
6.00
6.13
6.11
4.80
4.11
6.30
6.97
5.69
4.71
5.85
6.38
5.84
4.59
6.37
6.79
6.83
H
L

WAM WAVE MODEL